

# Forecasting Hurricane-forced Significant Wave Heights using the Long Short-Term Memory Network in the Caribbean Sea

Brandon J. Bethel<sup>1</sup>, Wenjin Sun<sup>1,2</sup>, Changming Dong<sup>1,2,3\*</sup>, Dongxia Wang<sup>4</sup>

<sup>1</sup> School of Marine Sciences, Nanjing University of Information Science and Technology, Nanjing 210044, China

<sup>2</sup> Southern Ocean Science and Engineering Guangdong Laboratory (Zhuhai), Zhuhai 519000, China

<sup>3</sup> Department of Atmospheric and Oceanic Sciences, University of California, Los Angeles, CA 90095, USA

<sup>4</sup> China State Shipbuilding Corporation (Chongqing) Haizhuang Windpower Equipment Co., Ltd., Chongqing 400021, China

\*Correspondence to: Changming Dong (cmdong@nuist.edu.cn)

**Abstract.** A Long Short-Term Memory (LSTM) neural network is proposed to predict hurricane-forced significant wave heights (SWH) in the Caribbean Sea (CS) based on a dataset of 20 CS, Gulf of Mexico, and Western Atlantic hurricane events collected from 10 buoys from 2010 – 2020. SWH nowcasting and forecasting are initiated using LSTM on 0-, 3-, 6-, 9-, and 12-hr horizons. Through examining study cases Hurricanes Dorian (2019), Sandy (2012), and Igor (2010), results illustrate that the model is well suited to forecast hurricane-forced wave heights, but also much more rapidly, at a significantly cheaper computational cost as compared to numerical wave models, and much lower required expertise. Forecasts are highly accurate with regards to observations. For example, Hurricane Dorian nowcasts had correlation (R), root mean square error (RMSE), and mean absolute percentage error (MAPE) values of 0.99, 0.16 m, and 2.6%, respectively. Similarly, on the 3-, 6-, 9-, and 12-hr forecasts, results produced R (RMSE; MAPE) values of 0.95 (0.51 m; 7.99%), 0.92 (0.74 m; 10.83%), 0.85 (1 m; 13.13%), and 0.84 (1.24 m; 14.82%), respectively. In general, the model can provide accurate predictions within twelve hrs ( $R \geq 0.8$ ) and errors can be maintained at under 1 m within six hrs of forecast lead time. However, the model also consistently over-predicted the maximum observed SWHs. From a comparison of LSTM with a third-generation wave model, Simulating Waves Nearshore (SWAN), it was identified that when using Hurricane Dorian as a case example, nowcasts were far more accurate with regards to the observations. This demonstrates that LSTM can be used to supplement, but perhaps not replace, computationally expensive numerical wave models for forecasting extreme wave heights. As such, addressing the fundamental problem of phase shifting and other errors in LSTM or other data-driven forecasting should receive greater scrutiny from Small Island Developing States. To improve models results, additional research should be geared towards improving single-point LSTM neural network training datasets by considering hurricane track and identifying the hurricane quadrant in which buoy observations are made.

**Keywords:** hurricanes; significant wave height; wave height forecasting; Long Short-Term Memory network; Hurricane

30 Dorian; Small Island Developing States; Caribbean Sea

## 31 **1. Introduction**

32 Ordinarily, momentum and mechanical energy are transferred to the ocean's surface from the overlying atmosphere, giving  
33 rise to the ubiquitous surface gravity waves. Under forcing by tropical cyclones (TC), these waves become extreme and pose  
34 significant risks to coastal communities. As such, the study of TC-induced extreme significant wave heights (SWH) is at the  
35 current forefront of research and is traditionally accomplished by using an array of numerical models (Shao et al., 2019; Chao  
36 et al., 2020; Hu et al., 2020). However, although hindcasting, nowcasting, and forecasting (Alina et al., 2019; Cecilio and  
37 Dillenburg, 2020) can be performed using these models, they are all disadvantaged in that they all require large investments in  
38 high-performance computing resources, technical and scientific expertise, and crucially, time. For the Small Island Developing  
39 States and coastal communities of the Caribbean Sea (CS) which have yet to significantly invest in numerical modeling  
40 capabilities, other computationally cost-effective measures are required for wave height predictions. Consequently, alternatives  
41 are high priority. Recent research into artificial intelligence (AI)-based methodologies have shown that these techniques are  
42 highly effective at forecasting wave properties with minor computational expense, even under TC-forced states (Qiao and  
43 Myers, 2020; 2021).

44 Demonstrating, Chen et al. (2021) constructed a random forest (RF) supervised learning classifier to generate a surrogate  
45 for the Simulating Waves Nearshore (SWAN) third-generation numerical model and reduced the required computational time  
46 by a factor of 100. Wu et al. (2020) considered a physics-based machine learning model in conjunction with an artificial neural  
47 network for predictions of SWH and peak wave period where wind forcing, and initial wave boundary conditions are considered  
48 as inputs. Campos et al. (2021) used RF to select wind and wave variables to enhance wave forecasts. They found that RF was  
49 able to select the best forecast only in very short ranges using inputs of SWH, wave direction and period. However, variable  
50 selection for longer forecasts (five days and above) was much less certain. Huang and Dong (2021) improved upon the short-  
51 term prediction of SWH by decomposing deterministic and stochastic components using a complete ensemble empirical mode  
52 decomposition (CEEMD) algorithm and recurrence quantification analysis. A similar study by Zhou et al. (2021a)  
53 demonstrated that combining EMD and the long short-term memory (LSTM) network could also reduce SWH forecasting  
54 errors in the CS.

55 These methods are also effective under TC conditions. Important for the present study, Chen et al. (2020) applied a machine  
56 learning method to perform probabilistic forecasting of typhoon-forced coastal wave heights and found that the model could,  
57 based on wave height data and an array of typhoon characteristics, generate the predicted confidence interval that enclosed  
58 observed wave heights. Meng et al. (2021) considered introducing a deep learning method for long-term predictions of TC-

59 forced nearshore wave heights. The bidirectional Gated Recurrent Unit network was identified as an effective model for real-  
 60 time and 24-hrs ahead predictions. Wei and Cheng (2020) developed a two-step wind-wave prediction model to predict wind  
 61 speed and wave height under typhoon conditions and compared results with a one-step approach. It was identified that deep  
 62 recurrent neural networks could be used for forecasting in either case, but the two-step approach was more effective. Zhou et  
 63 al. (2021b) used the convolutional-LSTM (ConvLSTM) network to predict TC-induced SWHs in the South China Sea and  
 64 found that up to a 12-hr forecast horizon, the correlation between forecasted values and observations could reach 0.94.

65 Recently, Bethel et al. (2021a) used LSTM to eliminate gaps in either surface wind speed or SWH by using one variable  
 66 as a predictand to forecast its counterpart. While mean states were the focus of that study, one hurricane was used to demonstrate  
 67 the methodology's effectiveness under extreme states. This study continues along that path to generate an LSTM-based forecast  
 68 model exclusively for hurricane-forced SWHs in the CS using a set of input variables. This is deemed important for assessing  
 69 and mitigating the risk of catastrophic losses in life and economic productivity due to hurricanes as seen most recently with the  
 70 September 1st, 2019, landfalling of Hurricane Dorian in The Bahamas.

71 The remainder of this paper is structured as follows. Section 2 describes the data and methodology employed. Section 3  
 72 presents the main findings of this study. Sections 4 and 5 provide a discussion and the conclusion, respectively.

## 73 2. Data and Methodology

### 74 2.1 Observational Data

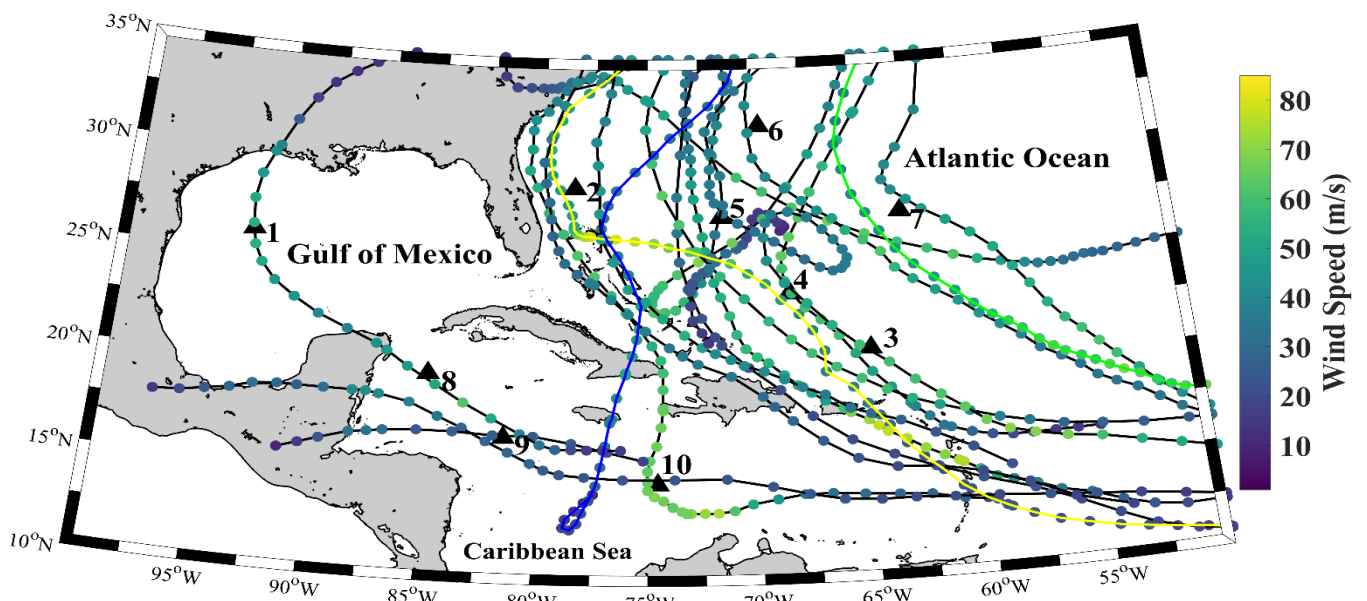
75 This study employs 10 buoys located throughout the CS, Gulf of Mexico, and Western Atlantic Ocean (Figure 1; Table 1)  
 76 that are owned and operated by the National Data Buoy Center (NDBC; <https://www.ndbc.noaa.gov/>). Acquired variables  
 77 include observations of surface wind speed and SWH. Gaps in buoy observations were processed using the insertion of  
 78 WaveWatch III reanalysis data acquired from the Pacific Islands Ocean Observing System (<https://coastwatch.pfeg.noaa.gov/>).  
 79 A total of twenty hurricanes identified from 2010 – 2020 were used and split into LSTM training and test datasets (Table 2).  
 80 Hurricane statistics were acquired from the hurricane database maintained by the National Hurricane Center  
 81 (<https://www.nhc.noaa.gov/>).

82 **Table 1. List of National Data Buoy Center buoys and their statistics.**

Buoy No.	Buoy ID	Latitude (°N)	Longitude (°W)	Anemometer Height (m)	Water Depth (m)
1	42002	26.055	93.64	3.8	3088
2	41010	28.878	78.485	4.1	890

3	41043	21.030	64.790	4.1	5362
4	41046	23.822	68.384	3.8	5549
5	41047	27.514	71.494	3.7	5321
6	41048	31.831	69.573	4.1	5394
7	41049	27.490	62.938	4.1	5459
8	42056	19.820	84.945	4.1	4554
9	42057	16.908	81.422	3.8	377
10	42058	14.776	74.548	3.8	4100

83 In some cases (e.g., Earl (2010), Igor (2010), Dorian (2019), Delta (2020)), the same hurricane was observed multiple  
84 times along its track. To increase the total length of the LSTM training/test sets, these data segments were arranged into a  
85 single time series. Additionally, cases such as Hurricane Humberto (2019) were explicitly excluded as swell contamination of  
86 the wave field could potentially lead to poor forecasts, despite its classification as a major hurricane, large effects on the marine  
87 environment (Avila-Alonso et al., 2021), and damage to the British overseas territory of Bermuda. Indeed, when a recently  
88 developed empirical wind-wave model for the CS was applied to Hurricane Humberto (2019) by Bethel et al. (2021b),  
89 observations of wind speed was a very poor predictor of the wave height and thus, given that surface wind speed and SWH are  
90 being used jointly here, worsening of LSTM predictions using Hurricane Humberto (2019) in the training dataset is natural.  
91 Unfortunately, it may not be possible to know a priori the existence of swell that may interfere with linear wind-wave  
92 relationships and as thus, this is a disadvantage of the current model.



93  
94 **Figure 1. Geographic map of the Caribbean Sea, Gulf of Mexico, and Western Atlantic Ocean with the best-tracks of each studied**  
95 **hurricane and National Data Buoy Center (NDBC) buoy locations (black triangles). Best-tracks from model training hurricanes are**

96 given in black, while the test best-tracks are given in yellow, blue, and green for Hurricanes Dorian, Sandy, and Igor, respectively.  
 97 Numbered from 1 – 10, the NDBC buoys employed are buoys 42002, 41010, 41043, 41046, 41047, 41048, 41049, 42056, 42057, and  
 98 42058, respectively.

99 **Table 2. Formation/dissipation dates, minimum air pressures and maximum wind speeds of the twenty hurricanes used in this study.**

Dataset	Hurricane (YYYY)	Formation Date (MM/DD)	Dissipation Date (MM/DD)	Minimum Air Pressure (hPa)	Maximum Wind Speed (m/s)
Training Set	Earl (2010)	8/25	9/5	927	63.8
	Irene (2011)	8/21	8/30	942	54.16
	Katia (2011)	8/29	9/12	942	61.1
	Ernesto (2012)	8/1	8/10	973	43
	Cristobal (2014)	8/23	9/2	965	38.8
	Gonzalo (2014)	10/12	10/20	940	63.8
	Bertha (2014)	8/1	8/16	998	36.1
	Joaquin (2015)	9/28	10/15	931	69.4
	Matthew (2016)	9/27	10/7	934	75
	Jose (2017)	9/5	9/25	938	69.4
	Maria (2017)	9/16	10/2	908	77
	Irma (2017)	8/30	9/14	914	79.16
	Florence (2018)	8/31	9/18	937	66.6
	Nana (2020)	9/1	9/4	994	33.3
	Teddy (2020)	9/12	9/24	945	66.1
	Delta (2020)	10/4	10/12	953	61.1
Isaias (2020)	7/30	8/5	986	41.6	
Test Set	Dorian (2019)	8/24	9/7	910	82.7
	Sandy (2012)	10/22	11/2	940	51.38
	Igor (2010)	9/8	9/23	924	69.4

100

101 **2.2 Methodology**

102 **2.2.1 The Long Short-Term Memory Network**

103 Originally developed by Hochreiter and Schmidhuber (1997), the LSTM network belongs to a class of recurrent neural

104 networks (RNNs). Along with its variants, LSTM has been widely used in forecasting and data reconstruction studies (Kim et  
 105 al., 2020; Bethel et al., 2021; Gao et al., 2021; Hu et al., 2021; Jörges et al., 2021). It has also been coupled with other machine  
 106 learning tools, neural networks, and numerical models (Choi and Lee, 2018; Ali and Prasad, 2019; Fan et al., 2020; Guan,  
 107 2020). LSTMs have an advantage over traditional feed-forward neural networks and other RNNs in that they can selectively  
 108 remember patterns in data. This is achieved by a series of forget ( $f_t$ ), input ( $i_t$ ), and output ( $o_t$ ) gates. Data passing through  
 109 these gates are processed using the sigmoid function ( $\sigma$ ) and the Hadamard product operator ( $\odot$ ; Yu et al., 2019). Each gate  
 110 may be computed as follows:

$$111 \quad f_t = \sigma(W_{xf}x_t + W_{hf}h_{t-1} + b_f) \quad (1)$$

$$112 \quad i_t = \sigma(W_{xi}x_t + W_{hi}h_{t-1} + b_i) \quad (2)$$

$$113 \quad o_t = \sigma(W_{xo}x_t + W_{ho}h_{t-1} + b_o) \quad (3)$$

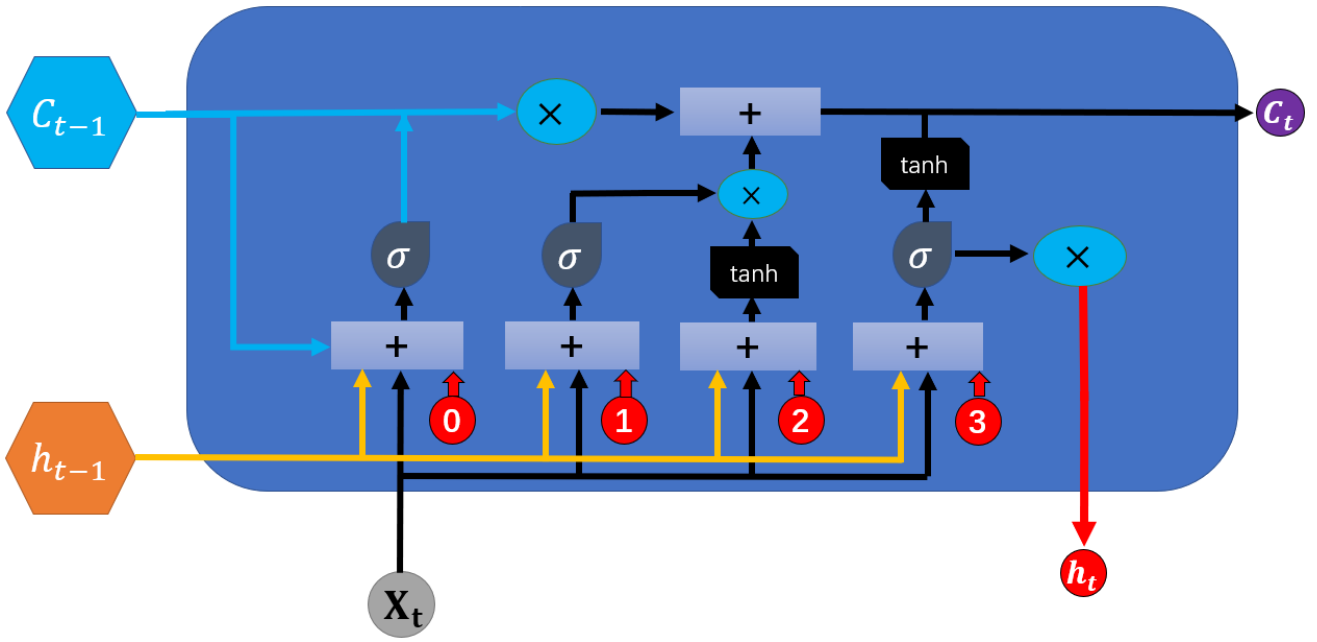
$$114 \quad g_t = \tanh(W_{xg}x_t + W_{hg}h_{t-1} + b_g) \quad (4)$$

$$115 \quad c_t = f_t \odot c_{t-1} + i_t \odot g_t \quad (5)$$

$$116 \quad h_t = o_t \odot \tanh(c_t) \quad (6)$$

117 where  $W$  is each layer's assigned weight,  $x_t$  is the input time step  $t$ ,  $b$  is the bias,  $c$  is the cell state, and  $\tanh$  is a hyperbolic  
 118 tangent function.

119 In sequence, the forget gate is used to delete past information where decisions on which information should be deleted is  
 120 defined as the value obtained from estimating the sigmoid following receiving  $h_{t-1}$  and  $x_t$ . The sigmoid function output  
 121 ranges from 0 to 1 so that if the value is 0, information of the previous state is completely deleted, and if 1, information is  
 122 completely preserved. The input gate saves current information and is processed alongside  $h_{t-1}$  and  $x_t$  before being applied  
 123 to the sigmoid function. The resulting information is then processed with the hyperbolic function and Hadamard product  
 124 operator before being sent out of the input gate. The strength and direction of information storage in the current cell is  
 125 represented by  $i_t$  and  $g_t$ , which respectively range from 0 to 1, and -1 to 1.



126  
127

**Figure 2. Architecture of the long short-term memory neural network cell.**

128 LSTM is set up with four layers that correspond to a time step of four. The recursive linear unit (ReLU) was used as the  
 129 activation function to maximize the model’s ability to capture nonlinearities. The Adaptive Moment Estimation (Adam)  
 130 optimizer is used to compute adaptive learning rates. The number of epochs was set to 100 and the batch size set to 3.  
 131 Throughout each experiment, the operating parameters were held constant. These settings were chosen after experiments (not  
 132 shown) as they produced the best results while avoiding overfitting. Similar settings can be found in Bethel et al. (2021a) and  
 133 Zhou et al. (2021a, 2021b). The data was partitioned along a 70/30 split into training and validation datasets. For clarification,  
 134 here, and only here, the word ‘dataset’ should be interpreted as a given test hurricane (the test set hurricanes of Table 2). A  
 135 general model is trained using the training set hurricanes of Table 2, but the model is specified to a given test set hurricane  
 136 using 70% of its time series, and the remaining 30% is used to validate the forecast.

### 137 2.2.2 Wind Speed Extrapolation

138 As seen in Table 1, no buoy measured wind speed at the standard 10 m height and thus, wind speeds were adjusted to this  
 139 height using the logarithmic wind profile:

$$140 U_{10} = U_x \frac{\ln(10/Z_0)}{\ln(x/Z_0)} \quad (7)$$

141 where  $U_x$  is the wind speed measured at a given buoy’s anemometer height,  $x$  is a given buoy’s anemometer height, and  $Z_0$   
 142 is the roughness length (0.0002; Golbazi and Archer, 2019).

143  
144  
145

### 146 2.2.3 Performance Indicators

147 Three commonly used statistical metrics: correlation coefficient (R), root mean square error (RMSE), and mean absolute  
148 percentage error (MAPE), are used to assess forecast efficacy. Their equations are as follows:

$$149 R = 1 - \frac{\sum_{i=1}^{N_i} (x_i - \bar{x}_i)(\hat{x}_i - \bar{\hat{x}}_i)}{\sqrt{\sum_{i=1}^{N_i} (x_i - \bar{x}_i)^2 \sum_{i=1}^{N_i} (\hat{x}_i - \bar{\hat{x}}_i)^2}}$$

$$150 RMSE = \sqrt{\frac{\sum_{i=1}^{N_i} (x_i - \hat{x}_i)^2}{N_i}} \quad (8)$$

$$151 MAPE = \frac{1}{N_i} \sum_{i=1}^{N_i} \left| \frac{x_i - \hat{x}_i}{x_i} \right| \times 100\%$$

152 where  $x_i$  and  $\hat{x}_i$  are the observed and forecasted SWH (m), respectively.  $N_i$  is the total number of observations and the  
153 overbar denotes averages.

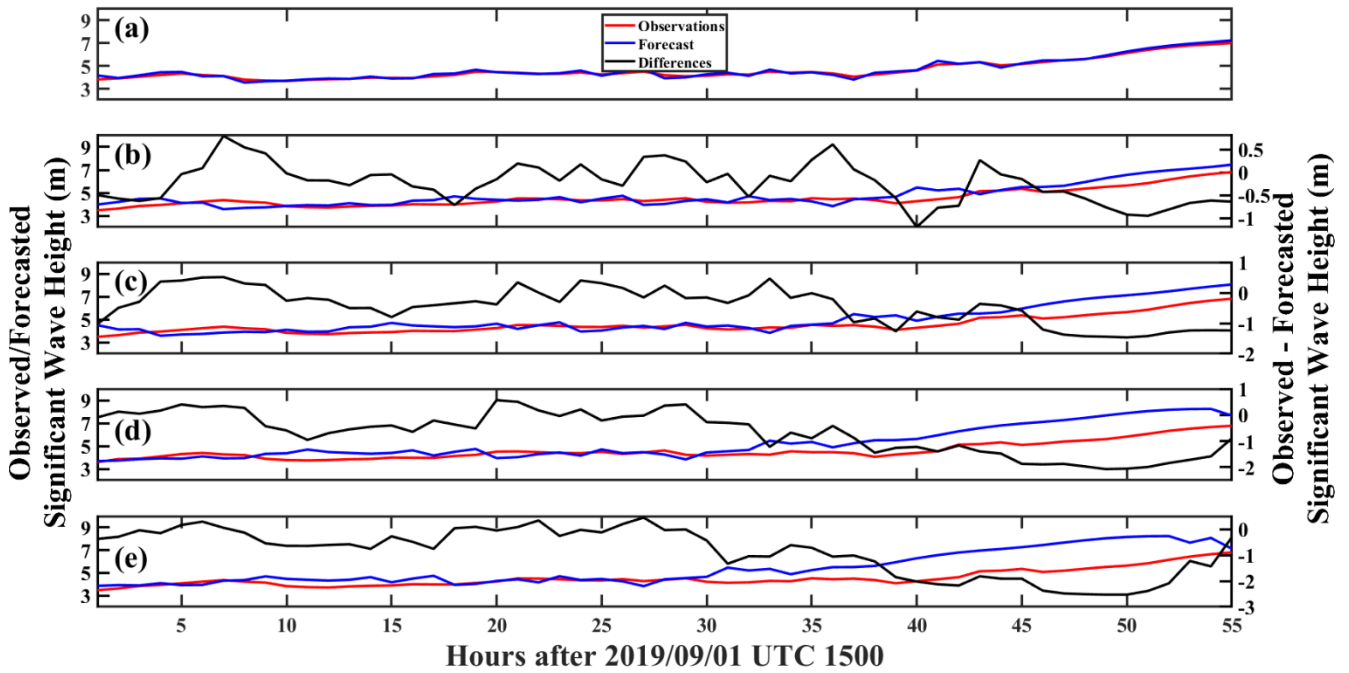
## 154 3. Results

### 155 3.1 Time Series Analysis

156 To evaluate forecast efficacy, time series of the observed and LSTM-forecasted, hurricane-forced SWHs for Hurricanes  
157 Dorian, Sandy, and Igor are given in Figures 3 – 5, respectively. Due to the lack of nearshore buoy observations within The  
158 Bahamas, no observations were made when Hurricane Dorian made landfall on Abaco island on September 1st, 2019. NDBC  
159 buoy 41010 nevertheless observed the growth of SWH under the influence of the hurricane several hundred kilometres away.  
160 In Fig. 3, time series of observed SWH was compared with the nowcast (0-hr, Fig. 3(a) and 3-, 6-, 9-, and 12-hr forecasts (Fig.  
161 3b-e, respectively). In Fig. 3a, it can be observed that an extremely tight fit between the forecasts and observations of Hurricane  
162 Dorian-forced SWHs at the start of wave growth from ~3.5 m to just under 7 m. However, at closer inspection, it can also be  
163 seen there are periods (e.g., at 42-hrs after UTC 1500 September 1) where the LSTM nowcast is unable to capture the extremely  
164 fine details. This is because in addition to errors introduced by LSTM's computations, there are also far too few examples of  
165 high-frequency components of the signal that the model could learn from and reproduce. Even following preprocessing using  
166 Empirical Mode Decomposition, high-frequency components of original SWH signals remain a challenge for LSTM (Zhou et  
167 al., 2021a). Nevertheless, this represents a discrepancy of far less than 1 m and is thus of very little importance when considering  
168 estimates of the wave state. When forecasts are performed on a 3-hr horizon, however, discrepancies between observations and  
169 the forecast have grown significantly larger where at different times, forecasted SWHs both underestimate and overestimate  
170 the observations. This phenomenon is especially noticeable at the 40- and 50-hrs after UTC 1500 September 1 marks. At the  
171 40-hr mark, SWHs were observed by buoy 41010 at approximately 5.5 m, but LSTM predicted a height of only approximately



172 4.2 m. The difference between the two clearly exceeds 1 m.

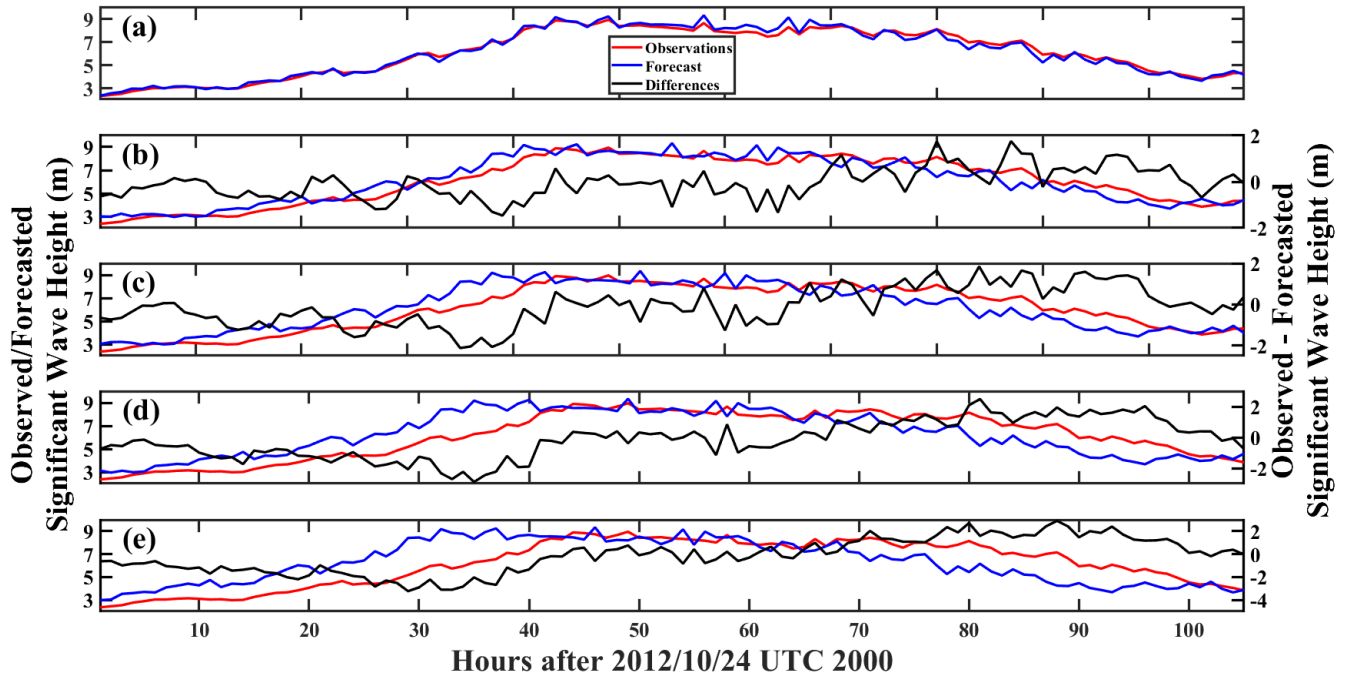


173  
 174 **Figure 3. Time series of Hurricane Dorian observed and LSTM-forecasted SWH (m) at the (a) 0-, (b) 3-, (c) 6-, (d) 9-, and (e) 12-hr**  
 175 **horizons, measured at buoy 41010.**

176 As total wave energy ( $P$ ) is extremely sensitive to SWH (i.e.,  $P \propto H_s^2 T_p$ , where  $H_s$  is the SWH and  $T_p$  is the wave period),  
 177 even minor underestimations of the wave height would lead to radically different energy output. Similarly, at the 50-hr mark,  
 178 SWH was measured at approximately 5.6 m, but LSTM forecasted a wave height of approximately 6.5 m. This overestimation  
 179 would produce the same radically different energy output than the observations. The same phenomenon can still be observed  
 180 for the 6-, 9- and 12-hr forecast horizons respectively presented in Fig. 6c-e, but at a significantly exacerbated scale. In each  
 181 case, at the tail end of the forecasts (35+ hrs after UTC 1500 September 1), the distance between the observations and forecasts  
 182 widened as the maximum wave height increased.

183 Identical to Hurricane Dorian, nowcasts of Hurricane Sandy were most efficient at reproducing the observations (Fig. 4a).  
 184 Interestingly, though there are some slight differences, LSTM was still able to capture finescale increases or decreases in SWH.  
 185 As the forecast horizon is extended to 3-hr in Fig. 4b, however, those finescale details were increasingly missed, though the  
 186 general wave growth and decay trends were captured. In Fig. 4c for the 6-hr forecast horizon, and before the 40-hr mark after  
 187 UTC 2000 September 10 mark, LSTM nearly consistently underestimated wave heights. Following this point at the peak of  
 188 the storm, LSTM virtually captured the observed SWH although finescale details were completely missed. During the wave  
 189 height decay stage, LSTM-forecasted wave heights overestimated the observations, but this discrepancy hovered at  $\sim 0.5$  m and  
 190 so, were not as extreme as the discrepancies seen during Hurricane Dorian at the same 6-hr forecast horizon (Fig. 3c). In Fig.  
 191 4d and 4e where the 9- and 12-hr forecast horizons are compared with observations, the differences between them is

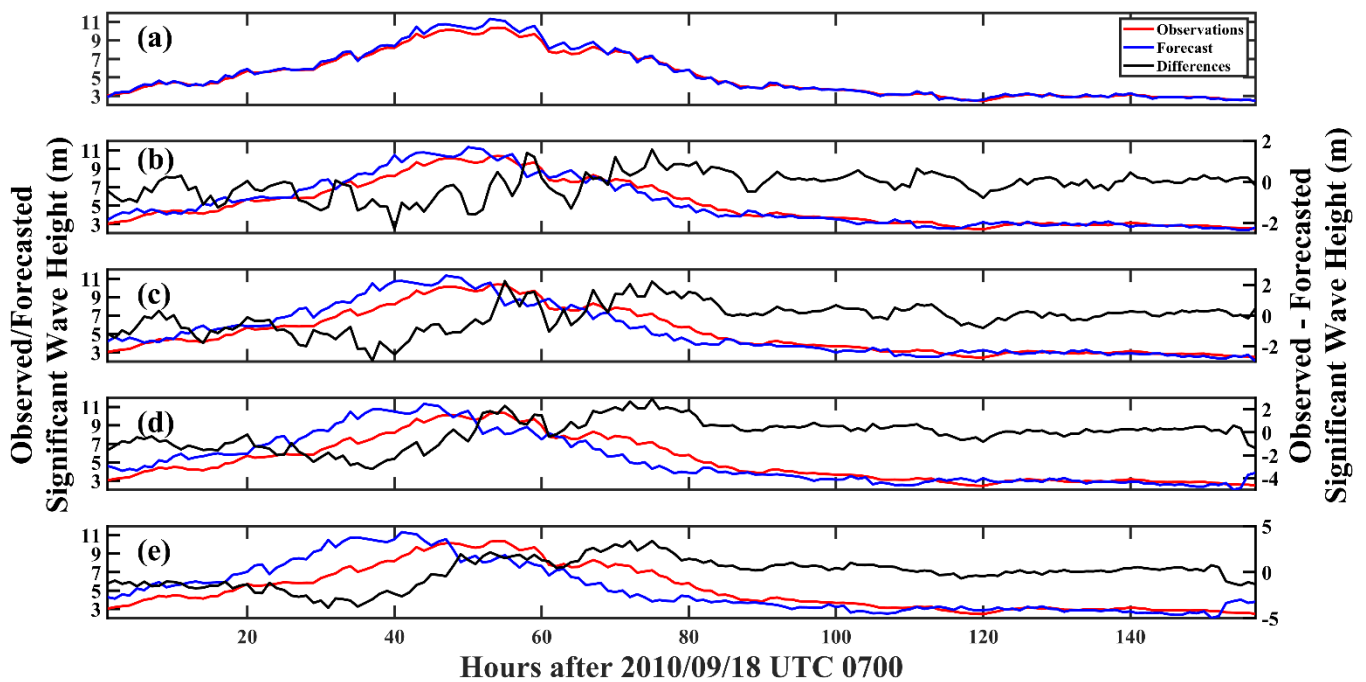
192 significantly larger than as compared to the 0-hr nowcast or the 3- and 6- hr forecast horizons of Fig. 4a-c.



193  
194 **Figure 4. Same as Figure 3, but for Hurricane Sandy (2012) measured at buoy 42058.**

195 At its most extreme, the difference between the forecasted (~6 m) and observed (~9 m) SWH reached a staggering 3 m  
196 at the 32-hr mark after UTC 2000 October 24. However, eight hrs later at the peak of the storm, LSTM was once again able to  
197 predict the observed SWHs more adequately. Although LSTM was able to capture the general decreasing, it largely  
198 overestimated the SWH as wave heights began to decrease with the passing of the storm. This overestimation was measured at  
199 approximately 2 m at the 90-hr mark after UTC 2000 October 24.

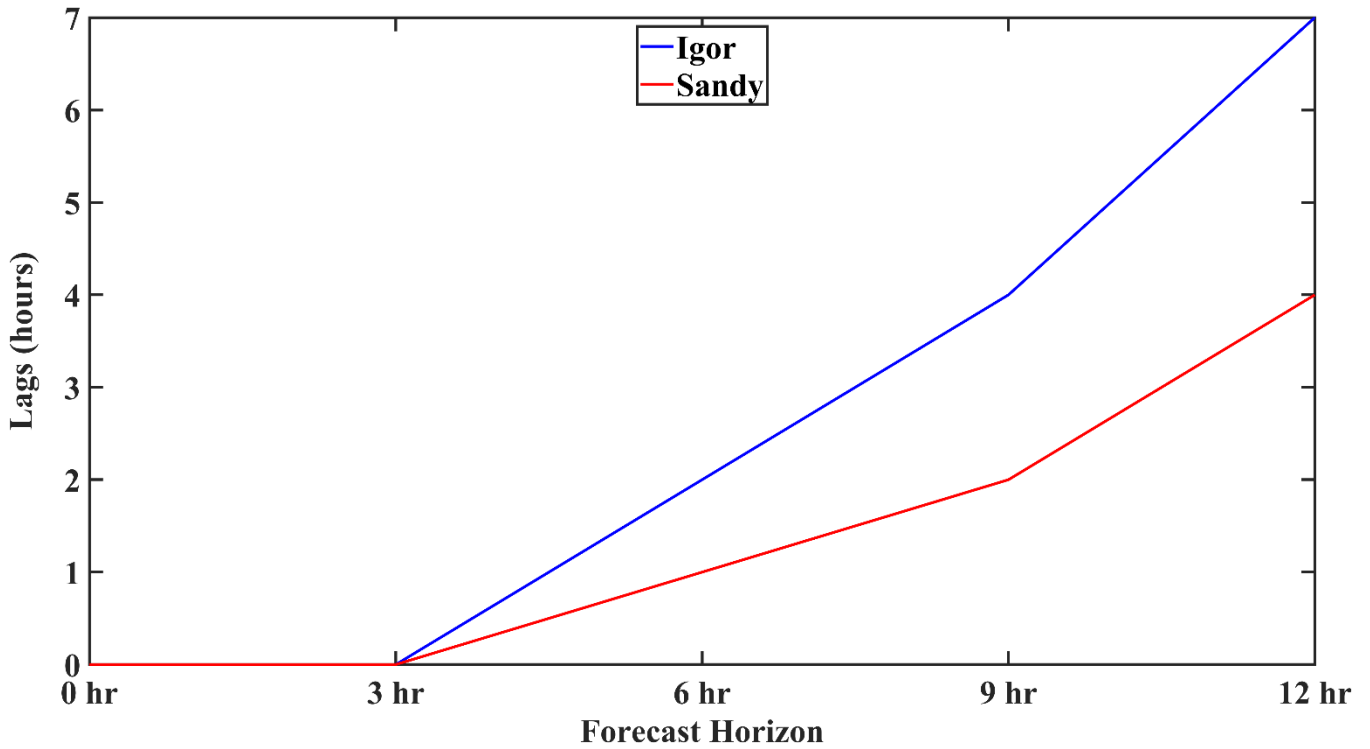
200 Although Hurricanes Dorian and Sandy, like Hurricane Igor, were extremely powerful systems, Igor however, spent most  
201 of its time in the Atlantic Ocean far away from any landmasses. Perhaps, then, the maximum wave height was allowed to grow  
202 to just under 11 m as an extremely long, uninterrupted fetch and duration would have been conducive for this wave growth.  
203 This is, of course, tempered by wind energy transfer rates and energy saturation of the wave field (Liu et al., 2008; Hwang and  
204 Fan, 2017; Babanin et al., 2019), in addition to balancing and decay by dissipative forces (Allahdadi et al., 2019; Rollano et  
205 al., 2019; Tamizi et al., 2021). In Fig. 5, similar to the previous two examples, the LSTM nowcast (Fig. 5a) produced  
206 exceptionally accurate results for Hurricane Igor (2010) with regards to the observations.



207  
 208 **Figure 5. Same as Figure 3, but for Hurricane Igor (2010) measured at buoys 41048 and 41049.**

209 This is even true at the peak of the storm at the 50-hr mark after UTC 0700 September 18 when wave heights reached a  
 210 maximum of just under 10 m. As the forecast horizon increased, however, the same pattern of forecast quality deterioration  
 211 could be observed where in Fig. 5b at the 3-hr horizon. Although LSTM was able to capture the general trend throughout the  
 212 time series, LSTM's predictions were slightly out of phase with the observations in its estimation of the point at which the  
 213 storm generated its maximum wave height (50 hrs after UTC 0700 September 18). This phenomenon becomes increasingly  
 214 apparent in the 6-hr (Fig. 5c), 9-hr (Fig. 6d) to the 12-hr (Fig. 5e) forecast horizons. Nevertheless, at the tail end of the time  
 215 series, regardless of the forecast horizon, LSTM produced highly accurate predictions of SWH under forcing by Hurricane Igor  
 216 (2010).

217 As the problem is most noticeable here, the problem of LSTM phase shifting during its time series forecasting will be  
 218 discussed. From Fig. 3, it should be identified that there are lags in forecasts as compared to the observation for Hurricane Igor.  
 219 This is also observable, but to a much smaller degree in Fig 4. for Hurricane Sandy. Consequently, autocorrelation between  
 220 time series were estimated and with lag results are presented in Fig. 6. Hurricane Dorian is not shown as its lags were all 0 for  
 221 each forecast horizon. There, it can be observed that for Hurricane Sandy, the lags increased from 0 hrs at the nowcast (0-hr)  
 222 and 3-hr forecast, to 1 hr at the 6-hr forecast and continued to increase to 4 hrs at the 12-hr forecast. Similarly, for Hurricane  
 223 Igor, there was also no lag between the time series from the nowcast (0-hr) and 3-hr forecast, but over time, lags gradually  
 224 increased from 2 hrs at the 6-hr forecast horizon, to up to 7 hrs at the 12-hr forecast horizon. This occurs because the farther in  
 225 time predictions are made, errors at each time step builds upon the previous prediction error, thus shifting forecast values.



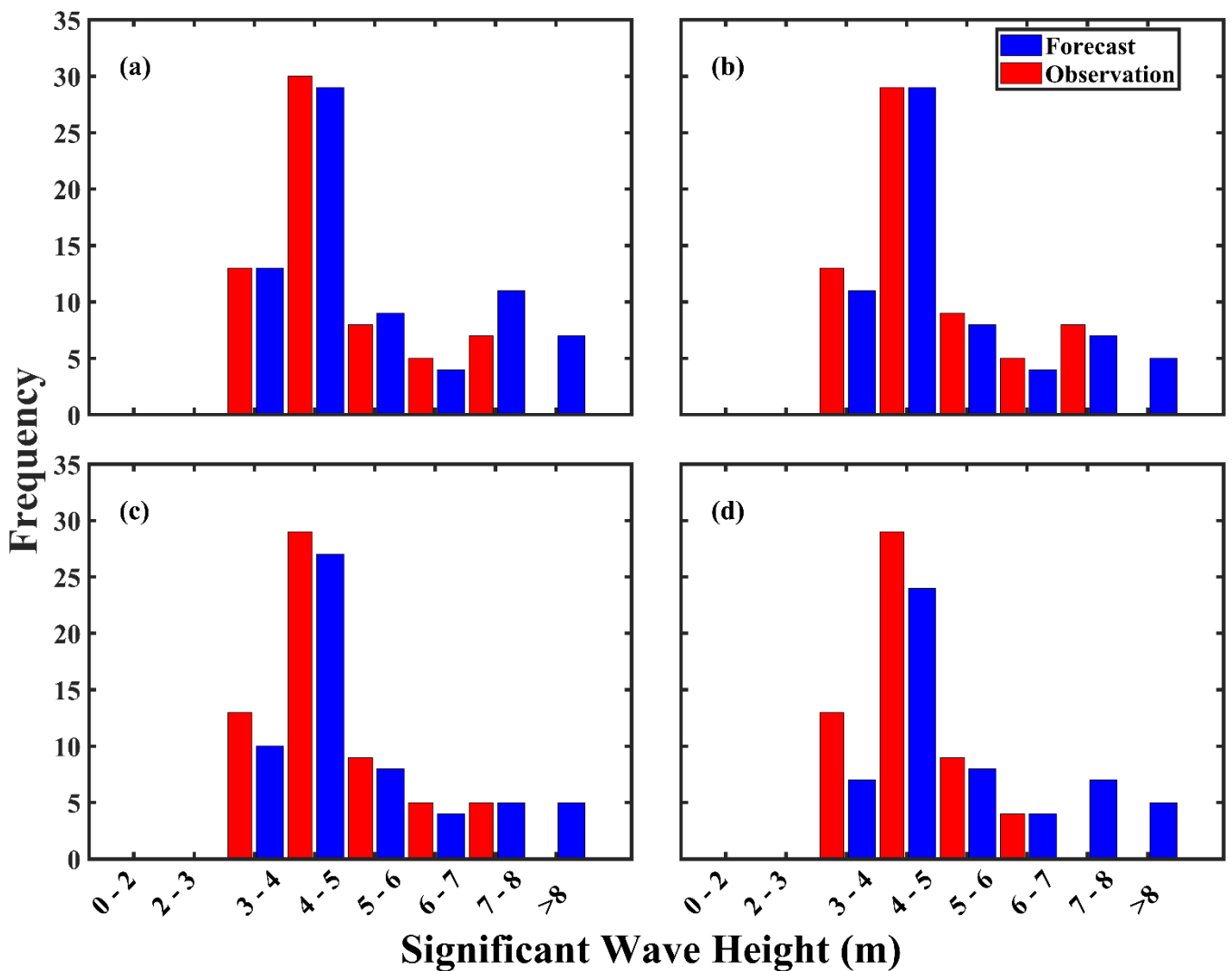
226  
227 **Figure 6. Estimated lags due to phase shifting of forecasted time series for Igor (blue) and Sandy (red).**

228 Curiously, the problem of phase shifting and increasing lags over forecast horizon time may also be related to the length  
229 of the time series for a given hurricane event. During experiments, it was noted that as the number of wave height events as  
230 recorded by a buoy during a hurricane increased, the severity of phase shifting also increased alongside observed lags. Data-  
231 driven methods such as LSTM, while they can learn and reproduce the relationships of a variety of climate variables and are  
232 therefore suitable for forecasting, they are prone to making phase shift errors, oscillations, and failures (Kaji et al., 2020;  
233 Morgenstern et al., 2021). Here, Hurricane Igor that possessed the longest time series and as such, its phase shift errors were  
234 most severe, leading to the largest lags between SWH forecast and observation time series. Unfortunately, this and other errors  
235 are inherent to LSTM and may require additional experimentation in modifying the input time series as Morgenstern et al.  
236 (2021) noted that structural changes to LSTM by the usage of encoder/encoder architectures or offsetting the start of forecasts  
237 to the forecast horizon of interest produced no noticeable positive change. While phase shifts and lags represent rather large  
238 disadvantages for this model as it will not be able to accurately predict the timing of, for example, maximum wave heights,  
239 this appears to be only a problem at extended forecast horizons (i.e., 6 hrs and beyond). Nevertheless, the lags are all well  
240 within 12 hrs and thus, although this model should not be depended upon to the exclusion of other forecasting methods, it can  
241 still give several hours of advance warning to coastal communities and regional governments to make minor changes to  
242 hurricane protection plans.

243

### 244 **3.2 Histogram Analysis**

245 Precise and not merely accurate estimates of hurricane-forced SWHs have the potential to enhance risk assessments and  
 246 mitigation strategies as these systems make landfall or approach offshore structures (Hatzikyriakou and Lin, 2017; Marsooli  
 247 and Lin, 2018; Masoomi et al., 2018; Guo et al., 2020; Song et al., 2020). This first section investigates the distribution of  
 248 forecasted SWHs in comparison with observations for hurricanes Dorian, Sandy, and Igor. In Fig. 7, histograms of observed  
 249 and forecasted SWHs under forcing by Hurricane Dorian is presented. In Fig. 7a, it can be observed that for the 0-hr SWH  
 250 nowcast, the model approximately exactly matched observations at the 3 – 4 m bin, but minutely underestimated the  
 251 observations at the subsequent 4 – 5 m bin. Alternating overestimations and underestimations occurred for the 5 – 6 m and 6 –  
 252 7 m bins, but unfortunately, overestimations were most severe at the >8 m bin. There, there were no observed occurrences of  
 253 wave heights over 8 m, but the model incorrectly predicted their existence.

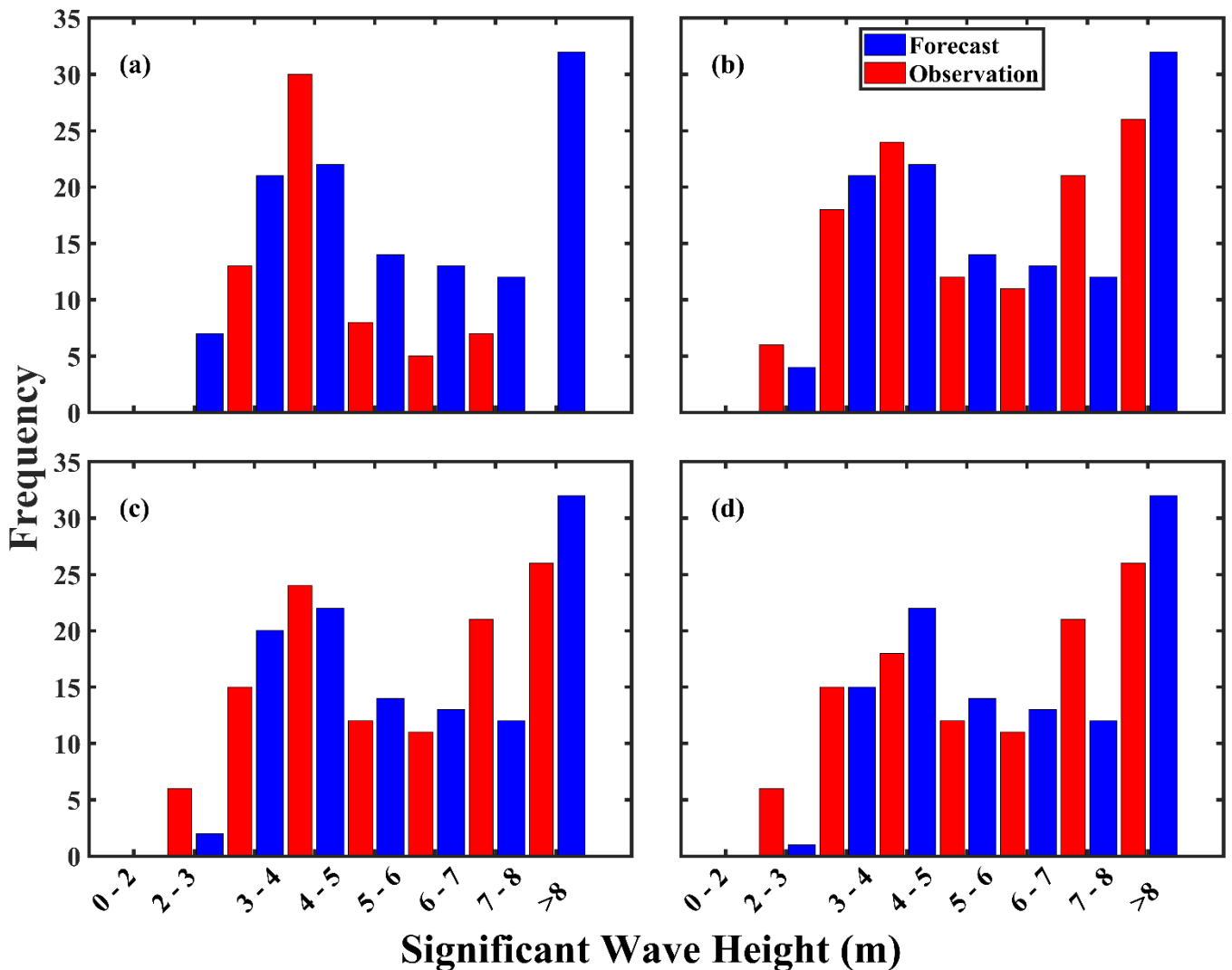


254  
 255 **Figure 7. Histograms of Hurricane Dorian observed (red) vs forecasted (blue) SWH (m) at the (a) 0-, (b) 3-, (c) 6-, and (d) 12-hr**  
 256 **forecast horizons. Results for the 9-hr forecast are presented in Figure S1.**

257 In Fig. 7b, relatively good agreement between the forecasted and observed SWHs, but discrepancies between them have  
 258 become increasingly apparent. Though at the 0-hr forecast in Fig. 7a forecasted and observed SWHs exactly matched, LSTM

259 underestimated the frequency of 3 – 4 m wave heights, but exactly matched the frequency of slightly higher (4 – 5 m) waves.  
 260 LSTM underestimations continued through the 6 – 8 m bins, but again, the model overestimated the frequency of waves higher  
 261 than 8 m. This trend remains consistent at the 6- and 9-hr forecasts in Fig. 7c and S1, but at the 12-hr forecast in 7d, excluding  
 262 the 6 – 7 m and >8 m bins where LSTM respectively exactly matched and overestimated the observations, underestimations of  
 263 the frequency of other wave heights occurred at all other bins.

264 Likewise, Fig 8. presents histograms of observed and nowcasted/forecasted SWHs as forced by Hurricane Sandy. In Fig.  
 265 4a, while the maximum wave heights forced by Hurricane Sandy (~9 m) exceeded that of Hurricane Dorian (~8 m), LSTM  
 266 was still able to adequately predict the wave height distribution. However, alternating patterns of under- and overestimations  
 267 of the frequency of wave heights can still be observed. In Fig. 8a, the 0-hr nowcast underestimated the observations from the  
 268 2 – 3 m up to the 4 – 5 m bins before abruptly overestimating all remaining bins, with the >8 m being the most severe case.

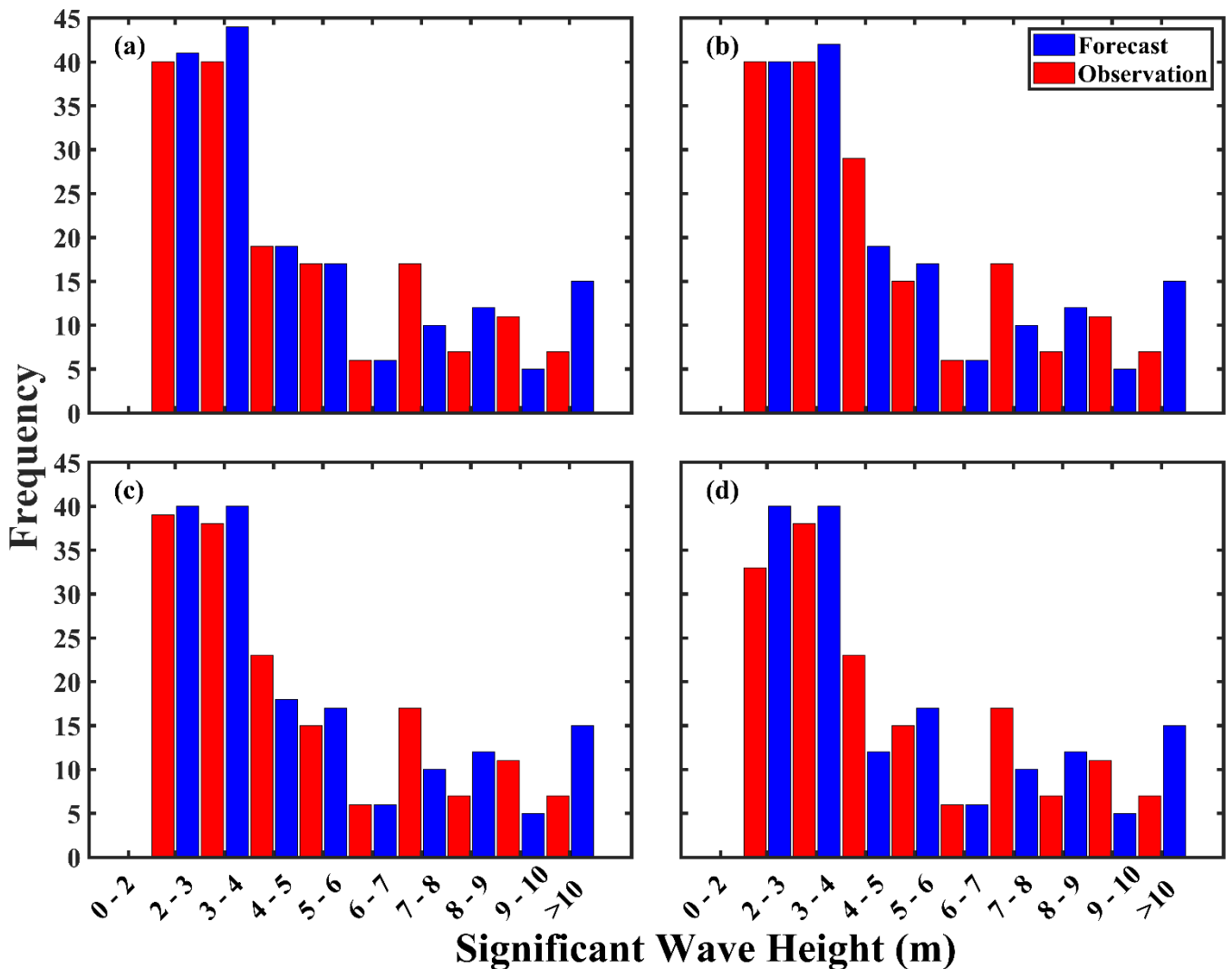


269  
 270 **Figure 8. Same as Figure 7, but for Hurricane Sandy. Results for the 9-hr forecast are presented in Figure S3.**

271 In Fig 8b at the 3-hr forecast horizon, results are largely improved over the 0-hr nowcast, but underestimations throughout

272 most of the wave height bins continue. The exception to this remains the overestimation of the frequency of the highest (i.e., >8  
 273 m) wave heights. The case remains the same for Figs. 8c, S3, and 8d at the 6-, 9-, and 12-hr forecast horizons.

274 Results for Hurricane Igor are presented in Fig. 9. Here, Igor produced SWHs that exceeded either Hurricanes Dorian or  
 275 Sandy, but interestingly, regardless of the forecast horizon, LSTM was able efficiently (but still imperfectly) forecast the wave  
 276 height distribution, even at wave heights up to 9 – 10 m. However, identical to the previous hurricane cases, the frequency of  
 277 maximum wave height predictions greater than 10 m is overestimated. Throughout the forecast horizons, naturally, the 0-hr  
 278 forecast produced the best results (Fig. 9a). Deterioration of the forecasted wave height frequency and magnitude increased  
 279 steadily from the 3-, 6-, 9-, and 12-hr forecast horizons as shown in Fig. 9b-c, S6, and 9d.



280  
 281 **Figure 9. Same as Figure 7, but for Hurricane Igor (2010). Results for the 9-hr forecast are presented in Figure S4.**

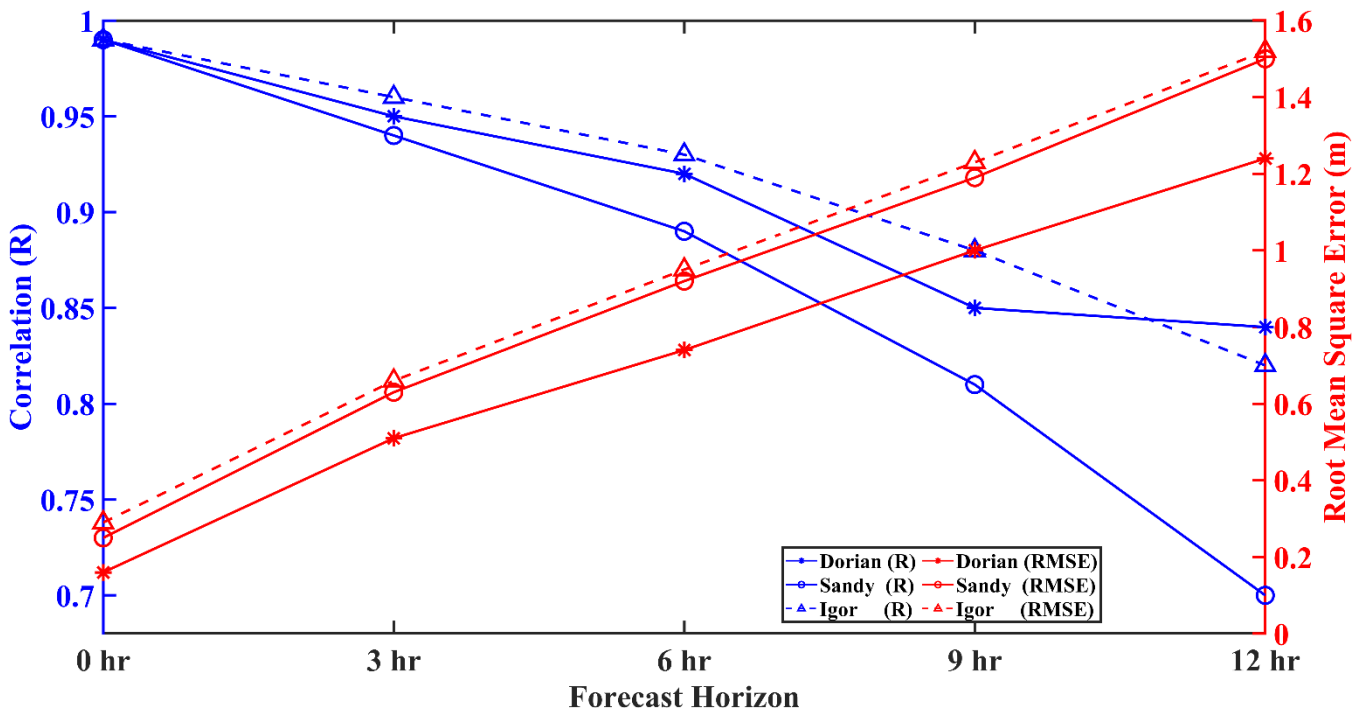
282 Consistent features of the model are its apparent under- and overestimation of both the frequency of wave heights, and  
 283 their magnitudes (Figures S2, S4, and S6). Specifically, the model can underestimate wave heights anywhere by 0.5 – ~2 m in  
 284 the cases of Dorian (Figure S2) and Sandy (Figure S6), but also overestimate heights by 2 – 3.5 m. With regards to Igor, this

285 phenomenon is even more severe with underestimations ranging from 0.5 – ~3 m, and overestimations reaching ~4 m. With  
286 regards to the overestimations, this may indicate that the training dataset contains too many examples of very high wave heights,  
287 which thus necessitates the inclusion of less powerful hurricanes for model training. Though counterintuitive, this is deemed  
288 required as wave growth under hurricane forcing is not merely a function of the maximum wind speed. Indeed, an array of  
289 factors which include, but are certainly not limited to the specific tracks, translation speed and environment (e.g., obstacles  
290 reducing fetch and duration), or modulating factors (e.g., surface currents) all have an impact on wave growth, maintenance,  
291 and decay (Drost et al., 2017; Zhang and Oey, 2018; Hegermiller et al, 2019). Thus, if less powerful hurricanes are considered  
292 in the training dataset as a control (i.e., minimizing the maximum wind speeds available to growth surface waves, regardless  
293 of environment or surface wave-modulating factors), the probability of preferentially populating the training set with large  
294 waves can be decreased. An added benefit would be the inclusion of low wave heights to aid in minimizing underestimation  
295 errors.

### 296 **3.3 Total Model Performance**

297 Overall forecast quality can be assessed through the statistical metrics of R, RMSE, and MAPE, with results for each  
298 hurricane illustrated graphically in Fig. The full range of statistics is available in Table 3. In Fig. 10, it can be observed that  
299 regardless of hurricane, model forecast effectiveness (R) hovered near a perfect 1, but naturally deteriorated over time. By the  
300 3-hr horizon, the three cases diverged from another in reflectance of each hurricane’s characteristics. By the 12-hr horizon, the  
301 model was able to maintain accuracies above 0.8 in the majority of cases, which demonstrates that the model remained highly  
302 effective at predictions over a 12-hr time frame. Errors are also minimal: within a 6-hr forecast, RMSEs in all cases can be  
303 maintained under 1 m, but this is increases to just under 1.6 m after a further six hours. Thus, it is suggested that short-range 0  
304 – 6-hr forecasts be prioritized over 12 hours when precision, rather than accuracy is required. Moreover, out of the hurricane  
305 cases, Hurricane Sandy’s R performance decreased more rapidly than either Hurricanes Dorian or Igor. This may be related to  
306 the hurricane’s track through the central Caribbean Sea (Figure 1). There, both the Caribbean Low-Level Jet (CLLJ) and  
307 Caribbean Current flow in the atmosphere and ocean, respectively.



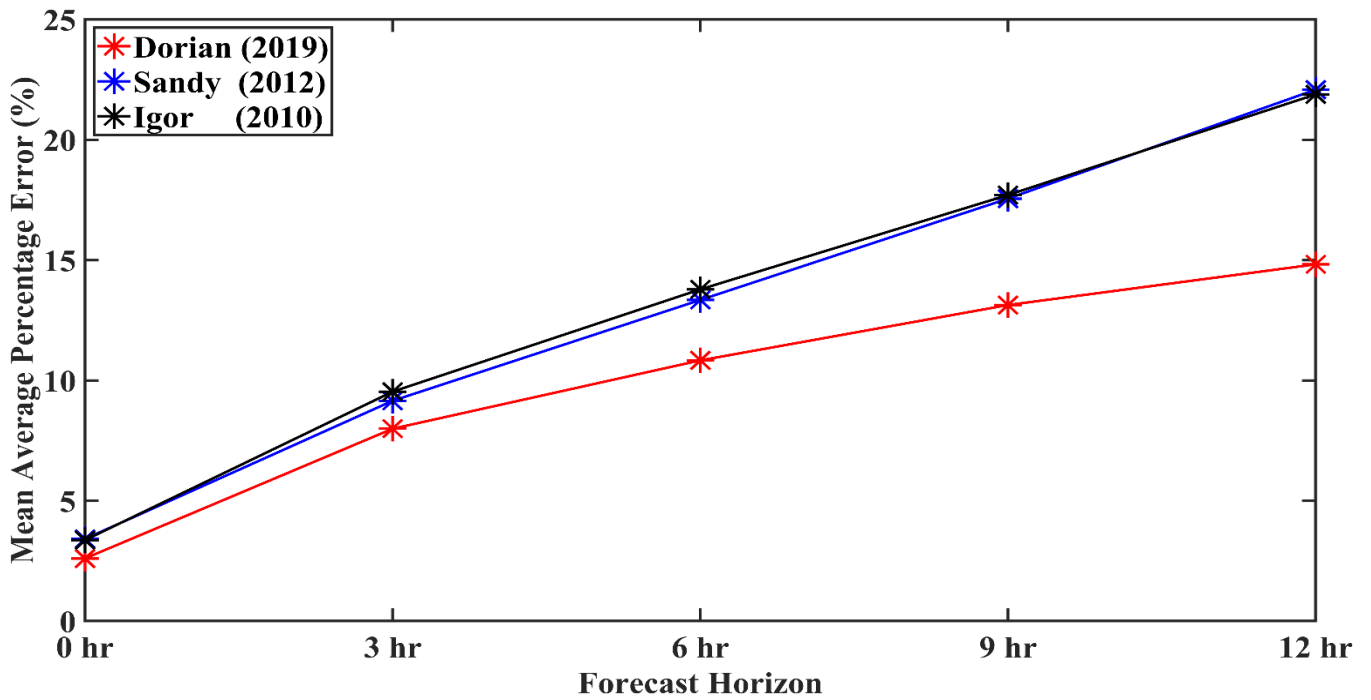


308

309 **Figure 10. LSTM model forecast performance in terms of R (blue) and RMSE (red) as compared with the observations for**  
 310 **Hurricanes Dorian, Sandy, and Igor.**

311 It is thought that rather than Sandy’s induced wave properties being affected by CLLJ which would have its normal zonal  
 312 (with the main axis at 15°N) flows disrupted by the hurricane itself, the Caribbean Current would undoubtedly have changed  
 313 hurricane-induced wave properties. Wave-current interactions have been widely demonstrated to change surface wave  
 314 properties in a variety of scenarios including, but not limited to tidal flows (Hopkins et al., 2015), large-scale current structures  
 315 such as the Loop Current and eddies (Romero et al., 2017), but as relevant for this discussion, also hurricane-induced wave  
 316 interactions with large-scale currents (Sun et al., 2018; Hegermiller, et al., 2019). Unfortunately, as NDBC buoy 42058 that  
 317 measured the passing of Sandy does not possess surface current information, this hypothesis cannot be tested using the available  
 318 dataset or possible wave-current effects on hurricane wave field prediction quantified. The rapid decrease in R observed for  
 319 Sandy could possibly be related to surface current-induced changes in the wave field not accounted for by the dual usage of  
 320 wind speed and wave height as LSTM predictors for the wave height predictand.

321 In Fig. 11, the MAPE for each of the hurricanes are given. There, it can be observed that Hurricane Dorian had MAPE  
 322 values of 2.6% at the 0-hr nowcast and values of 7.99%, 10.83%, 13.13%, and 14.82% respectively at the 3-, 6-, 9-, and 12-hr  
 323 forecast horizons. By contrast Hurricanes Sandy (Igor) had MAPE values of 3.41% (3.36%), 9.15% (9.53%), 13.34% (13.78%),  
 324 17.55% (17.70%), and 22.08% (21.88%) at the 0-, 3-, 6-, 9-, and 12-hr forecast horizons. Both Hurricanes Sandy and Igor had  
 325 MAPE values approximately 67% higher than that of Hurricane Dorian at the 12-hr horizon.



326  
327 **Figure 11. Mean average percentage error (%) for Hurricanes Dorian (red), Sandy (blue), and Igor (black).**

328 The difference in MAPE, in addition to the R and RMSE, may be due to the nature of Hurricane Dorian’s time series of  
 329 wave heights as the system approached NDBC buoy 41010 (Figure 1; Figure 3). Unlike Sandy or Igor where wave heights  
 330 gradually grew to a peak and then declined, Hurricane Dorian’s profile was far more gradual, allowing for LSTM to learn a  
 331 comparatively much simpler pattern for forecasting. Indeed, unique to Hurricane Dorian, waves induced by the system were  
 332 only observed after they would have affected and be affected by the Bahamas’ continental shelf and its northern islands. As is  
 333 well understood, islands induce extensive modulation of the oceanic wave field. The presence of islands may cause  
 334 modifications to wave spectra, reductions in wave heights, and triggering wave diffraction (Cao et al., 2018; Björkqvist et al.,  
 335 2019; Passaro et al., 2021; Violante-Carvalho et al., 2021). Additionally, as seen for Hurricane Joaquin (2015) by Sahoo et al.  
 336 (2018), nonlinear wave setup and setdown processes occur when the system interacted with The Bahamas’ varying coastal  
 337 bathymetry, slope, and arching coastlines, and these, in conjunction with Hurricane Dorian’s inherent properties (i.e., it’s  
 338 extremely slow translation speed of ~1.4 – 2 m/s), may have all played varying roles in the significantly lower variability in  
 339 the pattern of wave growth at NDBC buoy 41010.

340  
341  
342  
343  
344  
345

346 **Table 3. LSTM forecast performance for Hurricanes Dorian, Sandy, and Igor.**

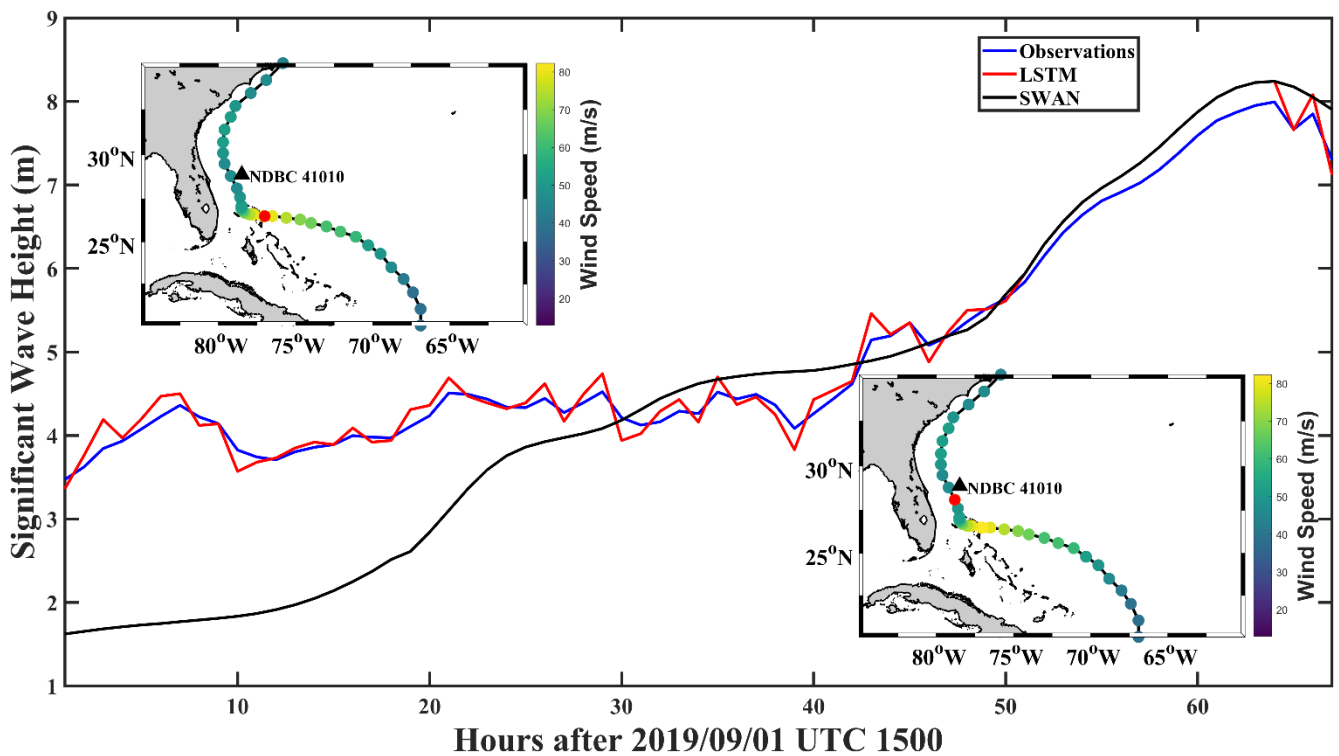
	R					RMSE (m)					MAPE (%)				
	Forecast Hour					Forecast Hour					Forecast Hour				
	0	3	6	9	12	0	3	6	9	12	0	3	6	9	12
Dorian	0.99	0.95	0.92	0.85	0.84	0.16	0.51	0.74	1.00	1.24	2.6	7.99	10.83	13.13	14.82
Sandy	0.99	0.94	0.89	0.81	0.70	0.25	0.63	0.92	1.19	1.51	3.14	9.15	13.34	17.55	22.08
Igor	0.99	0.96	0.93	0.88	0.82	0.29	0.66	0.95	1.23	1.52	3.36	9.53	13.78	17.70	21.88

### 347        **3.4 LSTM Model Comparison**

348        Under the influence of climate change, TCs are widely expected to occur more frequently and with greater ferocity (Chen  
349 et al., 2020; Kossin et al., 2020; Geiger et al., 2021). For the CS, the most recent and striking example of this phenomenon  
350 occurred during the September 1<sup>st</sup>, 2019, landfalling of Hurricane Dorian in The Bahamas (Zegarra et al., 2020), which, in  
351 addition to damage caused by extremely strong winds and storm surge, hurricane-forced SWHs more than likely added to the  
352 damage. Thus, predicting these and other hurricane-forced wave events is of extreme importance, but for Caribbean and other  
353 SIDS around the world, these predictions should be of the highest accuracy and where possible, precision, timely, and of  
354 minimum required computational expense and expertise (Bethel et al., 2021b). In Figure 12, a comparison is made between  
355 the LSTM nowcasted (0-hr) SWH from Figure 3a with SWAN simulations of the same period of time (for model description,  
356 see Bethel et al., 2021a), and the observations. Top right and bottom left insets present the position and wind speed of  
357 Hurricane Dorian at the start and end of the time series, respectively.

358        Primarily, the most significant feature in the comparison between SWAN-simulated and LSTM-nowcasted SWHs is that  
359 with regards to the observations, LSTM nowcasts are far more accurate at reproducing the time series than SWAN. At the  
360 start of the time series (up to ~30 hrs after 1500 UTC September 1<sup>st</sup>, 2019), the discrepancy between the LSTM nowcast and  
361 observations are minimal, while SWAN simulations suggest wave heights of just under 2 m, though observations are just  
362 over 3 m. This is remarkable as at that time, the storm was briefly stalled over The Bahamas but waves radiating out could  
363 still grow the SWH kilometres away at NDBC buoy 41010 to be recorded. With wind speeds reaching and exceeding 80 m/s,  
364 wave heights were just over twice the climatological mean. Following training by past hurricanes, LSTM nowcasts of  
365 Hurricane Dorian were very efficient at recreating the observed time series, but at this juncture, SWAN was very notably  
366 unable to do so. This may be potentially caused by the usage of low spatial resolution ( $0.5^\circ \times 0.5^\circ$ ) WaveWatch III reanalysis  
367 to fill in gaps in buoy data (the ‘observations’), thus leading to wide deviations from the SWAN-simulated SWH that  
368 possesses a significantly higher spatial resolution ( $0.2^\circ \times 0.2^\circ$ ). This phenomenon, however, should not be used to suggest  
369 SWAN simulations are inaccurate. Indeed, after the 30-hr mark following 1500 UTC September 1<sup>st</sup>, as Hurricane Dorian had  
370 migrated away from The Bahamas and decreased in intensity, SWAN’s capability at simulating SWHs dramatically increased,  
371 just as wave heights began to increase when the system’s distance (and maximum wind speeds) from buoy 41010 decreased.  
372 Here, though SWAN nevertheless overestimated wave height observations from 30 – 50 hrs after the start of the time series.  
373 Again, LSTM did a much better job at recreating the observations but interestingly, after this point, LSTM and SWAN exactly  
374 match one another, though they both overestimate the observations. This is a common feature between the data- and physics-

375 driven approaches at this time and to resolve them, two different approaches are required. Firstly, as previously identified,  
 376 the LSTM data-driven approach would require a few more examples of weaker storms to provide lower wave heights in the  
 377 training dataset, and this may have a beneficial effect on minimizing overestimations. The physics-based SWAN model, by  
 378 contrast, could be improved by advancing model-guiding physics (e.g., Aydoğan and Ayat, 2021), a better representation of  
 379 the wind field (Christakos et al., 2020) or online coupling with an atmospheric model such as the Weather Research and  
 380 Forecasting (WRF) model (Lim Kam Sian et al., 2020). It should be readily noted at this point that improving physics-based  
 381 models require far greater computational resources and expertise than does optimizing training sets for data-driven methods  
 382 such as LSTM.



383  
 384 **Figure 12. Comparison of SWH observations (blue), LSTM nowcast (red), and SWAN simulations (black) during (top left inset)**  
 385 **and after (bottom right inset) Hurricane Dorian's landfalling in The Bahamas. Red dots indicate the location of Hurricane Dorian**  
 386 **in either case.**

387 Demonstrating, a comparative analysis between LSTM and SWAN for SWH modeling is presented from the  
 388 perspectives of required model training/spinup and run times, in addition to their system and expertise requirements (Table  
 389 4). There, it can be noted that model training for LSTM took approximately 10 minutes, while for SWAN, model spinup took  
 390 just over half an hr. From there, LSTM forecasts took under a second to complete in a personal computer-based Python-  
 391 language integrated development environment (PyCharm), while the full run of SWAN took three hrs on two Xeon Gold

392 6152 CPU processors using a modest 56 cores. The SWAN run must also be understood in the context of the time and  
 393 expertise needed for preprocessing (i.e., preparing input wind fields, bathymetry, and boundary conditions), in addition to  
 394 considerations of further modeler skill and experience for processing and postprocess. Though SWAN allows for real-world  
 395 physics to be considered and thus the model can provide a far greater array of variables to a high degree of accuracy with  
 396 regards to observations, the CS and other SIDS around the world largely do not have either the required computational  
 397 resources or human resources to use these and other numerical models. Data-driven methods such as LSTM should therefore  
 398 be used to supplement existing forecasting tools considering their ease of use, accuracy, and low expertise and computational  
 399 resource requirements.

400 This study presented a 1D case, but the work here is easily extended to a 2D case as shown by Zhou et al. (2021b).  
 401 There, a ConvLSTM model was used on a GeForce RTX 2080 Ti graphics card for hurricane-forced SWH training and  
 402 forecasting. Very high accuracies with regards to a WaveWatch III baseline was achieved. Crucially, ConvLSTM model  
 403 training took only 2 hrs and forecasting took just under 20 seconds, which easily outperforms SWAN (here) in terms of speed,  
 404 and thus could be a viable alternative to the pure usage of numerical wave models under both mean and extreme (i.e., TC-  
 405 forced) wave conditions.

406 **Table 4. Model comparative analysis.**

Model	Training/Spinup Time (hr)	Model Run Time (hr)	Utilized Processor	Expertise Requirements
LSTM	1/6	<<1/60	Intel Core i7-10510U	Minor
SWAN	1/2	3	Xeon Gold 6152 CPU	Major

407

408 **4. Discussion**

409 Forecasting hurricane activity and its properties remains a daunting task for the scientific community, but great strides  
 410 have been made in the development of statistical/probabilistic methods, numerical models, and as presented in this study, AI  
 411 techniques. The results of this study are in strong agreement with those observed by Meng et al. (2021) and Wei (2021) that  
 412 each found that AI was highly effective at predicting hurricane-induced SWHs. However, although contemporary applications  
 413 of AI in the forecasting of both in mean and extreme (i.e., TC-forced) waves states have relied traditionally on singular inputs  
 414 of SWH (Ali and Prasad, 2019; Zhao and Wang, 2018; Zhou et al., 2021a, b), a growing body of literature have demonstrated  
 415 that the addition of other variables such as wind speed (as done here), wind direction and other variables improves forecast

416 effectiveness (Kaloop et al., 2020; Zubier, 2020; Raj and Brown, 2021; Wang et al., 2021). Uncertainties in variable selection  
417 have also stimulated research into how to best identify predictors for the SWH or other predictands (Li and Liu, 2020; Li et  
418 al., 2021). These results nevertheless remain consistent with the findings of Chen and Wang (2020) where the introduction  
419 of meteorological data could improve wave forecasts, but longer forecast horizons led to underestimations of extreme wave  
420 heights.

421 Moreover, discrepancies in forecasting outcomes between hurricanes in this study are slight, but noticeable. This may  
422 reflect differences in LSTM training and test hurricane properties. These include hurricane wind field, translation speed,  
423 approach angle and track which have been demonstrated to be essential factors in governing wave evolution (Zhang and  
424 Oey, 2018; Zhang and Li, 2019; Wang et al., 2020). For example, as a hurricane translated through the study area, wave  
425 properties in any of the four quadrants could have been measured by the chance intersection of the hurricane and its  
426 observing buoy (Zhang and Oey, 2018; Tamizi and Young, 2020; Tian et al., 2020; Collins et al., 2021). Thus, the model  
427 may have learned too much information from a particular quadrant. Consequently, when encountering a different  
428 quadrant in a forecasted hurricane, its results would naturally be poorer than if the model was trained solely on SWHs  
429 from quadrant A in training sets and forecasted quadrant A in the test set. Further experimentation would be required to  
430 identify the difference, if any, and magnitude of using data from a particular quadrant in a hurricane in the prediction of  
431 a different quadrant in a future hurricane. Other variables to consider, especially in the case of those hurricanes in the  
432 CS given its numerous islands, are the morphology of those islands as they can have a strong influence on local ocean  
433 dynamics (Cheriton et al., 2021). For those hurricanes that made landfall in The Bahamas, additional consideration  
434 should be given to the nonlinear interactions that hurricane waves and storm surge have on the archipelago's narrow  
435 and steep carbonate shelf and its variability due to elongated coastlines (Sahoo et al., 2019). These can perhaps be dealt  
436 with by the special application of a combination of a high order spectral method with Krylov subspace techniques as  
437 pioneered by Köllisch et al. (2018). Another set of examples come from Puerto Rico and the U.S. Virgin Islands (Joyce  
438 et al., 2019), and the shallow continental shelf between India and Sri Lanka (Sahoo et al., 2021). Consequently, training  
439 and test datasets certainly contain data from any of a hurricane's four quadrants, or in the case of Hurricanes Joaquin  
440 (2015) and Dorian data recorded along The Bahamas' vulnerable, eastern-most, Atlantic Ocean-facing islands. In these  
441 terms, the effect of training data selection on overall forecast quality has yet to be quantified and should be assessed.  
442 Following this, finescale LSTM-based hurricane-forced SWH forecast models for a given CS country or territory could  
443 potentially benefit from increased discrimination in selecting hurricane training data.

444 Accompanying increased scrutiny in building LSTM training datasets to improve predictions, the usage of physics-  
445 based/informed/infused versions of LSTM and other artificial intelligence and machine learning algorithms (Karniadakis et  
446 al., 2021; Zhang et al., 2021) may help to bridge the gap in forecasting efficacy between physics-based third-generation  
447 numerical wave models such as WaveWatch III or SWAN. Crucially, this will ensure that forecasting remains significantly  
448 computationally cheaper than the sole usage of wave models. These methods have been successfully applied to the solving  
449 of differential equations in engineering (Niaki et al., 2021; Zobeiry, and Humfeld, 2021), analyzing blood flow (Arzani et al.,  
450 2021), and chaotic systems (Khodkar and Hassanzadeh, 2021). Relevant for the current discussion, these methods are also  
451 finding use in weather and climate modelling (Kashinath et al., 2021). Considering the large physical complexities in wave  
452 evolution under TC forcing (Tamizi et al., 2021), and the many nonlinearities that govern crucial processes (Yim et al., 2017;  
453 Constantin, 2018; Sharifineyestani and Tahvildari, 2021), incorporating physics-informed, or knowledge-guided machine  
454 learning should, respectively, improve and lengthen forecast efficacy and horizons.

## 455 **5. Conclusion**

456 Precise, computationally cheap, and rapid SWH forecasting under hurricane forcing is of immense value to safeguard  
457 lives, property, and economic development in coastal communities and especially, SIDS. This study used surface wind speed  
458 and SWH forced by 17 hurricanes as input to the LSTM neural network to nowcast and forecast SWHs in the CS. Three  
459 hurricanes, Dorian (2019), Sandy (2012), and Igor (2010) were used as test cases. Results illustrated that the model was  
460 highly accurate at reproducing observed hurricane-forced wave height distributions both in terms of magnitude and frequency.  
461 However, there were discrepancies between observations and predictions. This was most easily observable from the  
462 comparison of observed and forecasted SWH time series for the three test cases.

463 In all cases, although the nowcasts naturally produced the best results, instances of slight under- and overestimations  
464 could nevertheless be observed at many finescale details. These under- and overestimations became more severe with  
465 increasing forecast horizon length. It has been demonstrated that wave height nowcasting (i.e., a forecast horizon of 0-hr)  
466 was very effective where in the test cases of Hurricanes Dorian (2019), Sandy (2012), and Igor (2010), R (RMSE) was  
467 measured at 0.99 (0.16 m), 0.99 (0.25 m), and 0.99 (0.29 m), respectively. Corresponding values of MAPE for Dorian, Sandy,  
468 and Igor were measured at 2.6%, 3.14%, and 3.36%, respectively. For forecast horizons ranging from 3-, 6-, 9-, and 12-hrs,  
469 with regards to observations, Dorian predictions produced R (RMSE; MAPE) values of 0.95 (0.51 m; 7.99%), 0.92 (0.74 m;  
470 10.83%), 0.85 (1 m; 13.13%) and 0.84 (1.24 m; 14.82%), respectively. Similarly, with regards to observations, Sandy  
471 predictions produced R (RMSE; MAPE) values of 0.94 (0.63 m; 9.15%), 0.89 (0.92 m; 13.34%), 0.81 (1.19 m; 17.55%) and



472 0.70 (1.51 m; 22.08%), respectively. Igor predictions produced R (RMSE; MAPE) values of 0.96 (0.66 m; 9.53%), 0.93 (0.95  
473 m; 13.78%), 0.88 (1.23 m; 17.70%) and 0.82 (1.52 m; 21.88%), respectively. In general, the model can provide forecasts with  
474 errors of 1 m within 6 hrs of lead time, and an accuracy of greater than 80% up to 12 hrs.

475 LSTM forecasts were also compared with a widely-used third generation model, SWAN in terms of model accuracy,  
476 computational expense, and difficulty of usage. Using Hurricane Dorian as an example, the data-driven LSTM model was,  
477 over the short-range nowcast, were far more accurate than SWAN. This is a trend widely observed in the literature (see  
478 Reikard and Rogers, 2011 for an excellent treatment on the subject). SWAN nevertheless was capable of simulating observed  
479 SWHs at the peak of the storm and here, achieved parity with LSTM for a brief period of time, demonstrating that within  
480 narrow windows, LSTM can provide accurate estimations of hurricane-forced wave fields, but crucially at a much faster pace  
481 and cheaper computational costs. Despite this, the study is limited in four significant ways.

482 Firstly, identical to Meng et al. (2021), this study focused on forecasting hurricane-forced SWHs, rather than mean states.  
483 Although a large number of hurricanes occurred over the study period, only a minority of these hurricanes were observed by  
484 buoys. Thus, the LSTM training datasets were severely limited in hurricane cases. This would have a significant effect on  
485 reducing forecast horizons and overall forecasting efficacy. A significantly expanded array of observational platforms in the  
486 Caribbean (i.e., both in situ buoys and remote sensing high-frequency coastal radars) would increase the likelihood of crucial  
487 hurricane wind/wave properties being observed in sufficiently high resolutions to make future research such as this possible.  
488 Secondly, and perhaps more importantly, as TCs and their properties rapidly evolve in space and time (Leroux et al., 2018;  
489 Bhalachandran et al., 2019; Chen et al., 2021), they naturally have great implications on the properties of waves they excite  
490 (Haryanto et al., 2021). If these properties change rapidly enough, LSTM alone would be unable to capture their  
491 characteristics. A recent study by Zhou et al. (2021b) demonstrated that an integrated EMD-LSTM model is more effective  
492 at forecasting rapidly evolving and large wave heights, but whether this remains true for hurricane-forced waves remains to  
493 be seen. Future research should investigate the efficacy of the EMD-LSTM model in forecasting hurricane-forced wave  
494 heights, and a ConvLSTM model fed with high-resolution wave data should be employed for two-dimensional hurricane-  
495 forced SWH. Thirdly, the selection of training and test sets would have an extremely strong impact on forecasting results.  
496 Specifically, Hurricanes Dorian, Sandy, and Igor were all far more powerful than hurricanes within the training set. These  
497 were chosen as it is expected that due to climate change, hurricanes are due to not only become more frequent, but also, more  
498 intense. The present method demonstrates that the model overestimates the highest SWHs of even those systems and should  
499 continue be effective if hurricanes become even more extreme (and thus, the degree by which the current model overestimates

500 maximum SWHs should decrease). However, if future systems are weaker than the test set (as it is now), the problem of  
501 overestimation would be exacerbated. Thus, a second model that is trained with hurricanes even weaker than the training set  
502 would be prudent and run in parallel to ensure both scenarios are considered in future disaster aversion strategies. Fourthly,  
503 LSTM-phase shifting of forecasted time series and resultant lags, seen most notably in Hurricanes Sandy and Igor, is a  
504 problem that needs to be rectified before the model can be used in real-world, operational TC wave forecasting applications.  
505 Extensive research into the mathematical principles underlying LSTM should be conducted by SIDS in the CS and around  
506 the world to realize low-cost but high-accuracy forecasts.

507 **Data Availability:** Buoy datasets are provided by the National Data Buoy Center and can be accessed at  
508 <https://www.ndbc.noaa.gov/>. Hurricane statistics can be acquired from the National Hurricane Center at  
509 <https://www.nhc.noaa.gov/>. WaveWatch III reanalysis data as provided by the Pacific Islands Observing System can be  
510 acquired at <https://coastwatch.pfeg.noaa.gov/>.

511

512 **Author Contributions:** BJB, WJS, CD and DXW designed the experiments and BJB carried them out. BJB developed the  
513 model code and performed the simulations. BJB prepared the manuscript with contributions from all co-authors.

514

515 **Acknowledgements:** The National Data Buoy Center is greatly thanked for the continued maintenance of its buoy array in  
516 the Caribbean and for ensuring the public accessibility of its data. The National Hurricane Center is thanked for providing  
517 the hurricane statistics and the Pacific Islands Ocean Observing System is thanked for providing WaveWatch III reanalysis  
518 data.

519

520 **Funding:** This work was supported by the Southern Marine Science and Engineering Guangdong Laboratory (Zhuhai)  
521 (SML2020SP007), the Innovation Group Project of the Southern Marine Science and Engineering Guangdong (Zhuhai) under  
522 contract No. 311020004, and the National Key Research and Development Program of China (2017YFA0604100,  
523 2016YFC1402004 and 2017YFC1404200).

524

525 **Competing Interests:** The authors declare that they have no conflict of interest.

526 **References**

- 527 Ali, M., and Prasad, R.: SWH forecasting via an extreme learning machine model integrated with improved complete  
528 ensemble empirical mode decomposition, *Renew. Sustain. Energy Rev.*, 104, 281-295,  
529 <https://doi.org/10.1016/j.rser.2019.01.014>, 2019.
- 530 Alina, A.I., Rusu, L., Catalin, A: Nearshore Wave Dynamics at Mangalia Beach Simulated by Spectral Models, *J. Mar. Sci.*  
531 *Eng.*, 7(7), 206, <https://doi.org/10.3390/jmse7070206>, 2019.
- 532 Allahdadi, M.D., He, R., Neary, V.S: Predicting ocean waves along the US east coast during energetic winter storms:  
533 sensitivity to whitecapping parameterizations, *Ocean Sci.*, 15(3), 617-715, <https://doi.org/10.5194/os-15-691-2019>, 2019
- 534 Arzani, A., Wang, J., D'Souza, R.M: Uncovering near-wall blood flow from sparse data with physics-informed neural  
535 networks, *Physics of Fluids*, 33(7): 071905, <https://doi.org/10.1063/5.0055600>, 2021.
- 536 Avila-Alonso, D., Baetens, J.M., Cardenas, R., De Baets, B: Oceanic response to the consecutive Hurricanes Dorian and  
537 Humberto (2019) in the Sargasso Sea, *Nat. Hazards Earth Syst. Sci.*, 21(2): 837-859, [https://doi.org/10.5194/nhess-21-837-](https://doi.org/10.5194/nhess-21-837-2021)  
538 2021, 2021.
- 539 Aydoğan, B., Ayat, B: Performance evaluation of SWAN ST6 physics forced by ERA5 wind fields for wave prediction in an  
540 enclosed basin. *Ocean Eng.*, 240:109936, <https://doi.org/10.1016/j.oceaneng.2021.109936>, 2021.
- 541 Babanin, A.V., Rogers, W.E., de Camargo, R: Waves and Swells in High Wind and Extreme Fetches, Measurements in the  
542 Southern Ocean, *Front. Mar. Sci.*, 6:361, doi: 10.3389/fmars.2019.00361, 2019.
- 543 Bethel, B.J., Dong, C., Zhou, S., Cao, Y: Bidirectional Modeling of Surface Winds and Significant Wave Heights in the  
544 Caribbean Sea. *J. Mar. Sci. Eng.*, 9(5), 547, <https://doi.org/10.3390/jmse9050547>, 2021a.
- 545 Bethel, B.J., Dong, C., Wang, J: An Empirical Wind-Wave Model for Hurricane-forced Wind Waves in the Caribbean Sea,  
546 *Earth Space Sci*, 8(12), e2021EA001956, <https://doi.org/10.1029/2021EA001956>, 2021b.
- 547 Bhalachandran, S., Nadimpalli, R., Osuri, K.K., Marks Jr., F.D., Gopalakrishnan, S., Subramanian, S., Mohanty, U.C., Niyogi,  
548 D: On the processes influencing rapid intensity changes of tropical cyclones over the Bay of Bengal. *Sci. Rep.*, 9, 3382,  
549 <https://doi.org/10.1038/s41598-019-40332-z>, 2019.
- 550 Björkqvist, J., Pettersson, H., Kahma, K.K: The wave spectrum in archipelagos. *Ocean Sci*, 15(6), 1469-1487,  
551 <https://doi.org/10.5194/os-15-1469-2019>, 2019.
- 552 Cao, Y., Dong, C., and Uchiyama, Y. et al: Multiple-Scale Variations of Wind-Generated Waves in the Southern California  
553 Bight. *J. Geophys. Res. Ocean*, 123(12), 9340-9356, <https://doi.org/10.1029/2018JC014505>, 2018.
- 554 Campos, R.M., Costa, M.O., Almeida, F., Guedes Soares, C: Operational Wave Forecast Selection in the Atlantic Ocean  
555 Using Random Forests. *J. Mar. Sci. Eng.*, 9(3), 298, <https://doi.org/10.3390/jmse9030298>, 2021.
- 556 Cecilio, R.O., Dillenburg, S.R: An ocean wind-wave climatology for the Southern Brazilian Shelf. Part 1: Problem  
557 presentation and model validation, *Dyn. Atmospheres Oceans*, 89: 101101, <https://doi.org/10.1016/j.dynatmoce.2019.101101>,  
558 2020.
- 559 Chao, Y., Huang, H., Wang, D., Liu, Y., Guo, Z: The Characteristics of Storm Wave Behavior and Its Effect on Cage Culture  
560 Using the ADCIRC+SWAN Model in Houshui Bay, China. *J. Ocean Univ. of China*, 19(2), 307-319, DOI: 10.1007/s11802-  
561 020-3941-3, 2020.

562 Chen, J, Wang, Z., Tam, C., Lau, N., Lau, D.D., Mok, H: Impacts of climate change on tropical cyclones and induced storm  
563 surges in the Pearl River Delta region using pseudo-global-warming method. *Sci Rep*, 10, 1965,  
564 <https://doi.org/10.1038/s41598-020-58824-8>, 2020.

565 Chen, T: Probabilistic forecasting of coastal wave height during typhoon warning period using machine learning methods,  
566 *Hydroinformatics*, 21(2), 343-358, <https://doi.org/10.2166/hydro.2019.115>, 2019.

567 Chen, S., Wang, Y: Improving Coastal Ocean Wave Height Forecasting during Typhoons by using Local Meteorological and  
568 Neighboring Wave Data in Support Vector Regression Models, *J. Mar. Sci. Eng.*, 8(3), 149,  
569 <https://doi.org/10.3390/jmse8030149>, 2020.

570 Chen, J., Pillai, A.C., Johannig, L., Ashton, I.: Using machine learning to derive spatial wave data: A case study for a marine  
571 energy site, *Environ. Model. Softw.*, 142: 105066, <https://doi.org/10.1016/j.envsoft.2021.105066>, 2021.

572 Chen, Y., Gao, S., Li, X., Shen, X: Key Environmental Factors for Rapid Intensification of the South China Sea Tropical  
573 Cyclones, *Front. Earth Sci.*, 8:609727, doi: 10.3389/feart.2020.609727, 2021.

574 Cheriton, O.M., Storlazzi, C.D., Rosenberger, K.J., Sherman, C.E., Schmidt, W.E: Rapid observations of ocean dynamics and  
575 stratification along a steep island coast during Hurricane María, *Sci. Adv.*, 7(20), DOI: 10.1126/sciadv.abf1552, 2021.

576 Choi, J.K., Lee, B: Combining LSTM Network Ensemble via Adaptive Weighting for Improved Time Series Forecasting,  
577 *Math. Probl. Eng.*, 2470171, <https://doi.org/10.1155/2018/2470171>, 2018.

578 Collins, C., Hesser, T., Rogowski, P., Merrifield, S: Altimeter Observations of Tropical Cyclone-generated Sea States: Spatial  
579 Analysis and Operational Hindcast Evaluation, *J. Mar. Sci. Eng.*, 9(2), 216, <https://doi.org/10.3390/jmse9020216>, 2021.

580 Constantin, A.: Nonlinear water waves: introduction and overview, *Philos. Trans. A Math. Phys. Eng. Sci.*, 376(2111), L  
581 20170310. doi: 10.1098/rsta.2017.0310, 2018.

582 Christakos, K., Furevik, B.R., Aarnes, O.J., Breivik, Ø., Tuomi, L., Byrkjedal, Ø: The importance of wind forcing in fjord  
583 wave modelling, *Ocean Dyn.*, 70, 57-75, <https://doi.org/10.1007/s10236-019-01323-w>, 2020.

584 Drost, E., Lowe, R., Ivey, G., Jones, N.L., Pequignet, C: The Effects of Tropical Cyclone Characteristics on the Surface Wave  
585 Fields in Australia's North West Region. *Cont. Shelf Res.*, 139, 35-53, <https://doi.org/10.1016/j.csr.2017.03.006>,  
586 2017.

587 Fan, S., Xiao, N., Dong, S: A novel model to predict SWH based on long short-term memory network, *Ocean Eng.*, 205:  
588 107298, <https://doi.org/10.1016/j.oceaneng.2020.107298>, 2020.

589 Gao, S., Huang, J., Liu, G, Bi, F., Bai, Z: A forecasting model for wave heights based on a long short-term memory neural  
590 network, *Acta Oceanologica Sinica*, 40, 62-69, <https://doi.org/10.1007/s13131-020-1680-3>, 2021.

591 Geiger, T., Gütshow, J., Bresch, D.N., Emmanuel, K., Frieler, K: Double benefit of limiting global warming for tropical  
592 cyclone exposure. *Nat. Clim. Chang*, 11, 861-866. <https://doi.org/10.1038/s41558-021-01157-9>, 2021.

593 Golbazi, M., Archer, C.L: Methods to Estimate Surface Roughness for Offshore Wind Energy, *Adv. Meteorol.*, 2019(2), 1-  
594 15, <https://doi.org/10.1155/2019/5695481>, 2019.

595 Guan, X.: Wave height prediction based on CNN-LSTM. 2020 2<sup>nd</sup> International Conference on Machine Learning, Big Data  
596 and Business Intelligence (MLBDBI), 23-25 Oct 2020, Taiyuan, China, DOI: 10.1109/MLBDBI51377.2020.00009, 2020.

597 Guo, Y., Hou, Y., Liu, Z., Du, M: Risk Prediction of Coastal Hazards Induced by Typhoon: A Case Study in the Coastal  
598 Region of Shenzhen, China, *Remote Sens.*, 12(11), 1731, <https://doi.org/10.3390/rs12111731>, 2020.

599 Hatziyriakou, A., Lin, N: Simulating storm surge waves for structural vulnerability estimation and flood hazard mapping,  
600 Nat. Hazard, 89, 939-962, <https://doi.org/10.1007/s11069-017-3001-5>, 2017.

601 Haryanto, Y.D., Riama, N.F., Purnama, D.R., Sigalingging, A.D: The Effect of the Difference in Intensity and Track of  
602 Tropical Cyclone on Significant Wave Height and Wave Direction in the Southeast Indian Ocean, The World Scientific  
603 Journal, 5492048, <https://doi.org/10.1155/2021/5492048>, 2021.

604 Hegermiller, C.A., Warner, J.C., Olabarreira, M., Sherwood, C.R: Wave-Current Interaction between Hurricane Matthew  
605 Wave Fields and the Gulf Stream, J. Phys. Oceanogr., 49(11), 2283-2900, <https://doi.org/10.1175/JPO-D-19-0124.1>, 2019.

606 Hochreiter, S., Schmidhuber, J: Long Short-term Memory, Neural Computation, 9(8), 1735-1780,  
607 <https://doi.org/10.1162/neco.1997.9.8.1735>, 1997.

608 Hopkins, J., Elgar, S., Raubenheimer, B: Observations and model simulations of wave-current interaction on the inner shelf.  
609 J. Geophys. Res. Ocean, 121(1), 198-208, <https://doi.org/10.1002/2015JC010788>, 2015.

610 Hu, Y., Shao, W., Wei, Y., Zuo, J: Analysis of Typhoon-Induced Waves along Typhoon Tracks in the Western North Pacific  
611 Ocean, 1998-2017, J. Mar. Sci. Eng., 8(7), 521, <https://doi.org/10.3390/jmse8070521>, 2020.

612 Hu, H., van der Westhuisen, A.J., Chu, P., Fujisaki-Manome, A: Predicting Lake Erie wave heights and periods using  
613 XGBoost and LSTM, Ocean Model., 164: 101832, <https://doi.org/10.1016/j.ocemod.2021.101832>, 2021.

614 Huang, W., Dong, S: Improved short-term prediction of SWH by decomposing deterministic and stochastic components,  
615 Renew. Energy, 177, 743-758. <https://doi.org/10.1016/j.renene.2021.06.008>, 2021.

616 Hwang, P.A., Fan, Y: Effective Fetch and Duration of Tropical Cyclone Wind Fields Estimated from Simultaneous Wind and  
617 Wave Measurements: Surface Wave and Air-Sea Exchange Computation, J. Phys. Ocean., 47(2), 447-470.  
618 <https://doi.org/10.1175/JPO-D-16-0180.1>, 2017.

619 Jörges, C., Berbenbrink, C., Stumpe, B: Prediction and reconstruction of ocean wave heights based on bathymetric data using  
620 LSTM neural networks, Ocean Eng., 232: 109046, <https://doi.org/10.1016/j.oceaneng.2021.109046>, 2021.

621 Joyce, B.R., Gonzalez-Lopez, J., Van der Westhuisen, A.J., Yang, D., Pringle, J., Westerink, J.J., Cox, A.T: U.S. IOOS Coastal  
622 and Ocean Modeling Testbed: Hurricane-Induced Winds, Waves, and Surge for Deep Ocean, Reef-Fringed Islands in the  
623 Caribbean, J. Geophys. Res. Ocean, 124(4), 2876-2907, <https://doi.org/10.1029/2018JC014687>, 2019.

624 Kaji, D., Watanabe, K., Kobayashi, M: Multi-Decoder RNN Autoencoder Based on Variational Bayes Method, 2020  
625 International Joint Conference on Neural Networks (IJCNN), July 19-24, 2020, 1-8, DOI:  
626 10.1109/IJCNN48605.2020.9206686, 2020.

627 Kaloop, M.R., Beshr, A.A.A., Zarzoura, F., Ban, W.H., Hu, J.W: Predicting lake wave height based on regression  
628 classification and multi input-single output soft computing models, Arab. J. Geosci., 13: 591, <https://doi.org/10.1007/s12517-020-05498-1>, 2020.

630 Karniadakis, G.E., Kevrekidis, I.G., Lu, L., Perdikaris, P., Wang, S., Yang, L: Physics-informed machine learning, Nat. Rev.  
631 Phys., 3, 422-440, <https://doi.org/10.1038/s42254-021-00314-5>, 2021.

632 Kashinath, K., Mustafa, M., Albert, A: Physics-informed machine learning: case studies for weather and climate modelling,  
633 Phil. Trans. R. Soc. A., 3792020009320200093. <http://doi.org/10.1098/rsta.2020.0093>, 2021.

634 Khodkar, M.A., Hassanzadeh, P: A data-driven, physics-informed framework for forecasting the spatiotemporal evolution of  
635 chaotic dynamics with nonlinearities modeled as exogenous forcing, J. Comput. Phys., 440: 110412,

636 <https://doi.org/10.1016/j.jcp.2021.110412>, 2021.

637 Kim, K., Lee, J., Roh, M., Han, K., Lee, G: Prediction of Ocean Weather Based on Denoising AutoEncoder and Convolutional  
638 LSTM, *J. Mar. Sci. Eng.*, 8(10), 805, <https://doi.org/10.3390/jmse8100805>, 2020.

639 Köllisch, N., Behrendt, J., Klein, M., Hoffmann, N: Nonlinear real time prediction of ocean surface waves, *Ocean Eng.*, 157,  
640 387-400, <https://doi.org/10.1016/j.oceaneng.2018.03.048>, 2018.

641 Kossin, J.P., Knapp, K.R., Olander, T.L., Velden, C.S: Global increase in major tropical cyclone exceedance probability over  
642 the past four decades. *PNAS*, 117(22), 11975-11980, <https://doi.org/10.1073/pnas.1920849117>, 2020.

643 Leroux, D., Wood, K., Elsberry, R.L., Cayan, E.O., Hendricks, E., Kucas, M., Otto, P., Rogers, R., Sampson, B., Yu, Z:  
644 Recent Advances in Research and Forecasting of Tropical Cyclone Track, Intensity, and Structure at Landfall, *Tropic.  
645 Cyclone Res. Rev.*, 7(2), 85-105, <https://doi.org/10.6057/2018TCRR02.02>, 2018.

646 Li, M., Liu, K: Probabilistic Prediction of SWH Using Dynamic Bayesian Network and Information Flow, *Water*, 12(8), 2075,  
647 <https://doi.org/10.3390/w12082075>, 2020.

648 Li, M., Zhang, R., Liu, K: A New Marine Disaster Assessment Model Combining Bayesian Network with Information  
649 Diffusion, *J. Mar. Sci. Eng.*, 9(6), 640, <https://doi.org/10.3390/jmse9060640>, 2021.

650 Lim Kam Sian, K.T.C., Dong, C., Liu, H., Wu, R., Zhang, R: Effects of Model Coupling on Typhoon Kalmaegi (2014)  
651 Simulation in the South China Sea, *Atmosphere*, 11(4):432, <https://doi.org/10.3390/atmos11040432>, 2020.

652 Liu, L.L., Wang, W., Huang, R.X: The Mechanical Energy Input to the Ocean Induced by Tropical Cyclones, *J. Phys. Ocean.*,  
653 38(6), 1253-1266, <https://doi.org/10.1175/2007JPO3786.1>, 2008.

654 Marsooli, R., Lin, N: Numerical Modeling of Historical Storm Tides and Waves and Their Interactions Along the U.S. East  
655 and Gulf Coasts, *J. Geophys. Res. Ocean*, 123, 3844-3874, <https://doi.org/10.1029/2017JC013434>, 2018.

656 Masoomi, H., van de Lindt, J.W., Ameri, M.R., Do, T., Webb, B: Combined Wind-Wave-Surge Hurricane-Induced Damage  
657 Prediction for Buildings, *J. Struct. Eng.*, 145(1), [https://doi.org/10.1061/\(ASCE\)ST.1943-541X.0002241](https://doi.org/10.1061/(ASCE)ST.1943-541X.0002241), 2018.

658 Meng, F., Song, T., Xu, D., Xie, P., Li, Y: Forecasting tropical cyclone wave height using bidirectional gated recurrent unit,  
659 *Ocean Eng.*, 234, 108795, <https://doi.org/10.1016/j.oceaneng.2021.108795>, 2021.

660 Morgenstern, T., Pahner, S., Mietch, R., Shütze: Flood forecasting in small catchments using deep learning LSTM networks.  
661 EGU General Assembly, EGU21-15072, <https://doi.org/10.5194/egusphere-egu21-15072>, 2021.

662 Niaki, S.A., Haghghat, E., Campbell, T., Poursartip, A., Vaziri, R: Physics-informed neural network for modelling the  
663 thermochemical curing process of composite-tool systems during manufacture, *Comput. Methods Appl. Mech. Eng.*, 384:  
664 113959, <https://doi.org/10.1016/j.cma.2021.113959>, 2021.

665 Passaro, M., Hemer, M.A., Quartly, G.D., et al: Global coastal attenuation of wind-waves observed with radar altimetry, *Nat.  
666 Commun*, 12(1):3812. <https://doi.org/10.1038/s41467-021-23982-4>, 2021.

667 Pushkarev, A.N., Zakharov, V.E: Nonlinear amplification of ocean waves in straits, *Theor. Math. Phys.*, 203, 535-546,  
668 <https://doi.org/10.1134/S0040577920040091>, 2020.

669 Pushpam, P.M.M., Enigo, F.V.S: Forecasting SWH using RNN-LSTM Models. 2020 4<sup>th</sup> International Conference on  
670 Intelligent Computing and Control Systems (ICICCS), 13-15 May 2020. Madurai, India,  
671 DOI: 10.1109/ICICCS48265.2020.9121040, 2020.

- 672 Qiao, C., Myers, A.T: Modeling Spatio-Temporal Characteristics of Metocean Conditions During Hurricanes Using Deep  
673 Neural Networks. ASME 2020 39<sup>th</sup> International Conference on Ocean, Offshore and Arctic Engineering, August 3-7,  
674 <https://doi.org/10.1115/OMAE2020-18989>, 2020.
- 675 Qiao, C., Myers, A.T: Surrogate modeling of time-dependent metocean conditions during hurricanes, *Nat. Hazards*,  
676 <https://doi.org/10.1007/s11069-021-05002-2>, 2021.
- 677 Raj, N., Brown, J: An EEMD-BiLSTM Algorithm Integrated with Boruta Random Forest Optimiser for SWH Forecasting  
678 along Coastal Areas of Queensland, Australia, *Remote Sens.*, 13(8), 1456, <https://doi.org/10.3390/rs13081456>, 2021.
- 679 Reikard, G, Rogers, W.E: Forecasting ocean waves: Comparing a physics-based model with statistical methods. *Coast. Eng.*,  
680 58(5), 409-416, <https://doi.org/10.1016/j.coastaleng.2010.12.001>, 2011.
- 681 Rollano, F.T., Brown, A., Ellenson, A: Breaking waves in deep water: measurements and modeling of energy dissipation,  
682 *Ocean Dyn.*, 69, 1165-1179, <https://doi.org/10.1007/s10236-019-01301-2>, 2019.
- 683 Romero, L., Lenain, L., Melville, W.K: Observations of Surface Wave-Current Interaction, *J. Phys. Ocean.*, 47(3), 615-632,  
684 <https://doi.org/10.1175/JPO-D-16-0108.1>, 2017.
- 685 Sahoo, B., Jose, F., Bhaskaran, P.K: Hydrodynamic response of Bahamas archipelago to storm surge and hurricane generated  
686 waves – A case study for Hurricane Joaquin, *Ocean Eng.*, 184, 227-238, <https://doi.org/10.1016/j.oceaneng.2019.05.026>,  
687 2019.
- 688 Sahoo, B., Sahoo, T., Bhaskaran, P.K: Wave-current-surge interaction in a changing climate over a shallow continental shelf  
689 region, *Reg. Stud. Mar. Sci.*, 46: 101910, <https://doi.org/10.1016/j.rsma.2021.101910>, 2021.
- 690 Shao, Z., Liang, B., Li, H., Li, P., Lee, D: Extreme SWH of tropical cyclone waves in the South China Sea, *Nat. Hazards*  
691 *Earth Syst. Sci.*, 19, 2067-2077, <https://doi.org/10.5194/nhess-19-2067-2019>, 2019.
- 692 Sharifineyestani, E., Tahvildari, N: Nonlinear Wave Evolution in Interaction with Currents and Viscoelastic Muds, *J. Mar.*  
693 *Sci. Eng.*, 9(5), 529, <https://doi.org/10.3390/jmse9050529>, 2021.
- 694 Song, H., Kuang, C., Gu, J., Zou, Q., Liang, H., Sun, X., Ma, Z: Nonlinear tide-surge-wave interaction at a shallow coast  
695 with large scale sequential harbor constructions, *Estuar. Coast. Shelf Sci.*, 233: 106543,  
696 <https://doi.org/10.1016/j.ecss.2019.106543>, 2020.
- 697 Sun, Y. Perrie, W., Toulany, B: Simulation of Wave-Current Interactions Under Hurricane Conditions Using an Unstructured-  
698 Grid Model: Impacts on Ocean Waves, *J. Geophys. Res. Ocean*, 123(5), 3739-3760, <https://doi.org/10.1029/2017JC012939>,  
699 2018.
- 700 Tamizi, A., Young, I.R: The Spatial Distribution of Ocean Waves in Tropical Cyclones, *J. Phys. Ocean.*, 50(8), 2123-2139,  
701 <https://doi.org/10.1175/JPO-D-20-0020.1>, 2020.
- 702 Tamizi, A., Alves, J., Young, I.R: The Physics of Ocean Wave Evolution within Tropical Cyclones, *J. Phys. Ocean*, 51(7),  
703 2373-2388, <https://doi.org/10.1175/JPO-D-21-0005.1>, 2021.
- 704 Tian, D., Zhang, H., Zhang, W., Zhou, F., Sun, X., Zhou, Y., Ke, D: Wave Glider Observations of Surface Waves During  
705 Three Tropical Cyclones in the South China Sea, *Water*, 12(5), 1331, <https://doi.org/10.3390/w12051331>, 2020.
- 706 Violante-Carvalho, N., Arruda, W.Z., Carvalho, L.M. et al: 2021: Diffraction of irregular ocean waves measured by altimeter  
707 in the lee of islands, *Remote Sens. Environ.*, 265(4):112653, <https://doi.org/10.1016/j.rse.2021.112653>, 2021.
- 708 Wang, X., Yao, C., Gao, G., Jiang, H., Xu, D., Chen, G., Zhang, Z: Simulating tropical cyclone waves in the East China Sea

709 with an event-based, parametric-adjusted model, *J. Ocean.*, 76, 439-457, <https://doi.org/10.1007/s10872-020-00555-5>, 2020.

710 Wang, J., Wang, Y., Yang, J: Forecasting of SWH Based on Gated Recurrent unit Network in the Taiwan Strait and Its Adjacent  
711 Waters, *Water*, 13(1), 86, <https://doi.org/10.3390/w13010086>, 2021.

712 Wei, C., Cheng, J: Nearshore two-step typhoon wind-wave prediction using deep recurrent neural networks,  
713 *Hydroinformatics*, 22(2), 346-367, <https://doi.org/10.2166/hydro.2019.084>, 2020.

714 Wei, Z: Forecasting wind waves in the US Atlantic Coast using an artificial neural network model: Towards an AI-based  
715 storm forecast system, *Ocean Eng.*, 237: 109646, <https://doi.org/10.1016/j.oceaneng.2021.109646>, 2021.

716 Wu, M., Stefanakos, C., Gao, Z: Multi-Step-Ahead Forecasting of Wave Conditions Based on a Physics-Based Machine  
717 Learning (PBML) Model for Marine Operations, *J. Mar. Sci. Eng.*, 8(12), 992, <https://doi.org/10.3390/jmse8120992>, 2020.

718 Yim, S.C., Osborne, A.R., Mohtat, A: Nonlinear Ocean Wave Models and Laboratory Simulation of High Seastates and  
719 Rogue Waves. Proceedings of the ASME 2017 International Conference on Ocean, Offshore and Arctic Engineering,  
720 OMAE2017, June 25-30, 2017. Trondheim, Norway, <https://doi.org/10.1115/OMAE2017-62706>, 2017.

721 Yu, Y., Si, X., Hu, C., Zhang, J: A Review of Recurrent Neural Networks: LSTM Cells and Networks, *Neural Comput.*, 31,  
722 1235-1270, [https://doi.org/10.1162/neco\\_a\\_01199](https://doi.org/10.1162/neco_a_01199), 2019.

723 Zegarra, M.A., Schmid, J.P., Palomino, L, Seminario, B: Impact of Hurricane Dorian in the Bahamas: A View from the Sky,  
724 Washington, D.C.: Inter-American Development Bank, 2020.

725 Zhang, L., Oey, L: An Observational Analysis of Ocean Surface Waves in Tropical Cyclones in the Western North Pacific  
726 Ocean, *J. Geophys. Res.: Ocean*, 124(1), 184-195, <https://doi.org/10.1029/2018JC014517>, 2018.

727 Zhang, C., Li, C: Effects of hurricane forward speed and approach angle on storm surges: an idealized numerical experiment.  
728 *Acta. Oceanol. Sin.*, 38, 48-56. <https://doi.org/10.1007/s13131-018-1081-z>, 2019.

729 Zhang, Z., Rai, R., Chowdhury, S., Doermann, D: MIDPhyNet: Memorized Infusion of Decomposed Physics in Neural  
730 Networks to Model Dynamic Systems, *Neurocomputing*, 428, 116-129, <https://doi.org/10.1016/j.neucom.2020.11.042>, 2020.

731 Zhao, K., Wang, J: SWH forecasting based on the hybrid EMD-SVM method, *Indian J. Geo Mar. Sci.*, 48(12), 1957-1962,  
732 2018.

733 Zhang, L., Oey, L: An Observational Analysis of Ocean Surface Waves in Tropical Cyclones in the Western North Pacific  
734 Ocean. *J. Geophys. Res. Oceans*, 124(1), 184-195, 2018.

735 Zhou, S., Bethel, B.J., Sun, W., Zhao, Y., Xie, W., Dong, C: Improving SWH Forecasts Using a Joint Empirical Mode  
736 Decomposition-Long Short-Term Memory Network, *J. Mar. Sci. Eng.*, 9, 744, 2021a.

737 Zhou, S., Xie, W., Lu, Y., Wang, Y., Zhou, Y., Hui, N., Dong, C: ConvLSTM-Based Wave Forecasts in the South and East  
738 China Seas, *Front. Mar. Sci.*, 8:680079. doi: 10.3389/fmars.2021.680079, 2021b.

739 Zobeiry, N., Humfeld, K.D: A physics-informed machine learning approach for solving heat transfer equation in advanced  
740 manufacturing and engineering applications, *Eng. Appl. AI*, 101: 104232, <https://doi.org/10.1016/j.engappai.2021.104232>,  
741 2021.

742 Zubier, K: Using an Artificial Neural Network for Wave Height Forecasting in the Red Sea, *Indian J. Geo Mar. Sci.*, 49(2),  
743 184-191, 2020.